



Including ash in UKESM1 model simulations of the Raikoke volcanic eruption reveals improved agreement with observations

Alice F. Wells¹, Andy Jones², Martin Osborne², Lilly Damany-Pearce¹, Daniel G. Partridge¹, and James M. Haywood^{1,2}

¹Department of Mathematics and Statistics, Faculty of Environment, Science and Economy, University of Exeter, Exeter, EX4 4QE, United Kingdom

²Met Office, Exeter, EX1 3PB, United Kingdom

Correspondence: Alice F. Wells (afw207@exeter.ac.uk)

Received: 7 October 2022 – Discussion started: 26 October 2022

Revised: 22 February 2023 – Accepted: 8 March 2023 – Published: 4 April 2023

Abstract. In June 2019 the Raikoke volcano, located in the Kuril Islands northeast of the Japanese archipelago, erupted explosively and emitted approximately $1.5 \text{ Tg} \pm 0.2 \text{ Tg}$ of SO_2 and 0.4–1.8 Tg of ash into the upper troposphere and lower stratosphere. Volcanic ash is usually neglected in modelling stratospheric climate changes since larger particles have generally been considered to be short-lived particles in terms of their stratospheric lifetime. However, recent studies have shown that the coagulation of mixed particles with ash and sulfate is necessary to model the evolution of aerosol size distribution more accurately. We perform simulations using a nudged version of the UK Earth System Model (UKESM1) that includes a detailed two-moment aerosol microphysical scheme for modelling the oxidation of sulfur dioxide (SO_2) to sulfate aerosol and the detailed evolution of aerosol microphysics in the stratosphere. We compare the model with a wide range of observational data. The current observational network, including satellites, surface-based lidars, and high-altitude sun photometers means that smaller-scale eruptions such as Raikoke provide unprecedented detail of the evolution of volcanic plumes and processes, but there are significant differences in the evolution of the plume detected using the various satellite retrievals. These differences stem from fundamental differences in detection methods between, e.g. lidar and limb-sounding measurement techniques and the associated differences in detection limits and the geographical areas where robust retrievals are possible. This study highlights that, despite the problems in developing robust and consistent observational constraints, the balance of evidence suggests that including ash in the model emission scheme provides a more accurate simulation of the evolution of the volcanic plume within UKESM1.

1 Introduction

Throughout history large explosive volcanic eruptions have resulted in periodic perturbations to the climate. Explosive volcanic eruptions frequently emit a combination of gases, including sulfur dioxide (SO_2) and volcanic ash, into the UTLS (upper troposphere–lower stratosphere) where the SO_2 oxidises, resulting in the formation of secondary sulfate aerosols. Sulfate aerosols in the stratosphere have a residence time of several months to a few years (e.g. Robock,

2000; Langmann, 2014; Jones et al., 2017) due to limited wet- and dry-deposition rates (Kloss et al., 2021). Sulfate aerosols are primarily reflective and enhance the scattering of shortwave solar radiation, increasing the albedo of the planet, and thus exert a cooling effect on the Earth's climate system (e.g. Robock, 2000; Gordeev and Girina, 2014). The extent of their impact upon the climate is dependent on a multitude of parameters, including the magnitude of the emission, location of the volcano, the injection altitude, and the composition of the plume (e.g. Jones et al., 2017).

In June 1991 Mount Pinatubo injected an estimated 10–20 Tg of SO₂ into the lower stratosphere (Bluth et al., 1992; Dhomse et al., 2014), causing potentially the largest aerosol perturbation to the stratosphere in the 20th century and resulting in average global lower-tropospheric temperatures cooling by around 0.5 °C across a period of nearly 2 years (McCormick et al., 1995; Guo et al., 2004). Whilst there has not been another volcanic eruption since Pinatubo to have such a significant impact on the global climate in subsequent years, there have been a series of more moderate eruptions. Kasatochi in Alaska erupted in August 2008, injecting an estimated 0.9–2.7 Tg of SO₂ (Corradini et al., 2010; Kravitz et al., 2010; Karagulian et al., 2010). The following year in June 2009, Sarychev Peak in the Kuril Islands was estimated to have injected 1.2 ± 0.2 Tg (Haywood et al., 2010), and Nabro in Eritrea erupted injected around 1.3–1.5 Tg of SO₂ in June 2011 (Clarisse et al., 2012). These eruption estimates for the three volcanic eruptions were later refined using a consistent algorithm: 0.9, 1.5, and 0.5 Tg loadings were derived above 10 km using the Michelson Interferometer for Passive Atmospheric Sounding (MIPAS) on Envisat (Höpfner et al., 2015). Haywood et al. (2014) estimate that over the period 2008–2012 these smaller volcanic eruptions contributed between –0.02 and –0.03 K of cooling at the Earth's surface.

While these volcanic eruptions injected an order of magnitude less SO₂ into the stratosphere than Pinatubo, monitoring the transport, evolution, and dispersion of volcanic plumes allows an assessment of the performance of global climate models in representing stratospheric sulfate plumes and allows improvements to be made in key processes. The much-improved observational network compared to that which observed the Pinatubo eruption, which includes satellite observations of both SO₂ (e.g. Cai et al., 2022) and sulfate aerosol (Lee et al., 2009), surface-based lidars (e.g. Chouza et al., 2020), high-altitude sun photometers (e.g. Toledano et al., 2018), and periodic balloon-borne observations (e.g. Jégou et al., 2013), means that observations of these smaller-scale eruptions provide unprecedented detail of the evolution of volcanic plumes and processes. The validation and improvement of representation of volcanic plumes within global climate models leads to a better understanding of their associated cooling impacts. Such synergy between observations and models also provides a means to assess the uncertainties associated with proposed stratospheric aerosol injection climate intervention strategies that have recently been suggested as a method to ameliorate the worst impacts of climate change (e.g. Lawrence et al., 2018).

This study examines the impact of the 2019 eruption of Raikoke. Almost exactly a decade after the eruption of Sarychev Peak (12 June 2009, 48.1° N, 153.2° E), on 21 June 2019 at 18:00 UTC, a neighbouring volcano – Raikoke (48.3° N, 153.2° E) – started to erupt, generating a series of distinct explosive events and emitting a plume of ash and SO₂ into the stratosphere. During this period,

it is estimated that it injected around 1.5 ± 0.2 Tg of SO₂ (Muser et al., 2020; Kloss et al., 2021; De Leeuw et al., 2021) and 0.4–1.8 Tg of ash (Bruckert et al., 2022) into the stratosphere, signifying the largest volcanic emission of SO₂ since the Nabro eruption in 2011. The resultant volcanic aerosol plume was detected at altitudes ranging between 11 to 20 km by the TROPOMI instrument (Hedelt et al., 2019; Vaughan et al., 2021) and at similar altitudes by other satellite instruments (e.g. Gorkavyi et al., 2021; Kloss et al., 2021), although altitudes as high as 26 km have been inferred in isolated lidar measurements (e.g. Chouza et al., 2020). These findings indicate that a significant portion of the volcanic plume was injected into the stratosphere. Gorkavyi et al. (2021) found that the peak sulfate aerosol extinction occurred around 1.5 months after the eruption date with an SO₂ *e*-folding lifetime of approximately 19 d. Previous studies looking at similar volcanic eruptions have found SO₂ *e*-folding times at a similar scale. For example, once the retrieval minimum detection threshold had been accounted for, Haywood et al. (2010) determined an *e*-folding for SO₂ from the Infrared Atmospheric Sounding Interferometer (IASI) for the Sarychev Peak eruption of around 20–22 d.

Less than a week after the eruption of Raikoke, a second volcanic eruption occurred – Ulawun (5.1° S, 151.3° E) – on 26 June 2019 and again on 3 August 2019. It is estimated to have injected around 0.14 Tg SO₂ into the stratosphere during the first explosive eruptive phase and a further 0.2 Tg SO₂ during the second phase of the eruption (Kloss et al., 2021).

The Raikoke and Ulawun eruptions were both well observed by a series of satellite instruments and ground-based measurement stations. Satellite observations include the Ozone Mapping Profiler Suite (OMPS) Nadir Mapper (NM) (Yang, 2017) and Limb Profiler (LP) (Taha, 2020) and the Cloud-Aerosol Lidar with Orthogonal Polarization (CALIOP) (Winker et al., 2009), while surface observations include those from high-altitude AEROSOL ROBOTIC NETWORK sites (AERONET; Holben et al., 1998). Although the perturbations to the Earth's radiation budget and near-surface temperature from moderate volcanic eruptions, such as Raikoke, are unlikely to be detectable owing to the small signal-to-noise ratio, these impacts can be estimated from Earth system models. The Raikoke eruption was the largest volcanic stratospheric injection of SO₂ since the OMPS satellite was launched in late 2011, providing an excellent opportunity to assess the skill and the limitations of the UK Earth System Model (UKESM1; Sellar et al., 2019) in simulating the evolution of the atmospheric distributions of SO₂ and sulfate aerosol.

Recent studies have drawn attention to the influence of ash on self-lofting and the evolution of the volcanic plume (e.g. Muser et al., 2020; Kloss et al., 2021). Volcanic ash is usually neglected in the modelling the impact of eruptions on the stratosphere and climate since larger particles (radii $r > 1 \mu\text{m}$) would be shorter lived owing to their considerable fall speed (Niemeier et al., 2021, 2009; Stenchikov et al., 2021). How-

ever, Zhu et al. (2020) showed that to produce the evolution of the size distribution following the Kelud eruption in 2014, the coagulation of internally mixed ash and sulfate particles is necessary. They also found that after this eruption super-micrometre-sized ash particles with an estimated density (0.5 g cm^{-3}) corresponding to pumice were the main component of the volcanic aerosol layer. This is in contrast to the assumed density ($\sim 2.3 \text{ g cm}^{-3}$) of ash within current models. Including ash emissions in model simulations has been found to alter the dynamics of sulfate aerosol formation (Shallcross et al., 2021; Stenchikov et al., 2021) including prolonging the lifetime of stratospheric aerosol optical depth (sAOD) (Kloss et al., 2021). Stenchikov et al. (2021) and Abdelkader et al. (2023) agreed that when modelling the Pinatubo eruption, including volcanic ash increases the radiative heating during the first week after the eruption and results in the lofting of the aerosol.

Muser et al. (2020) examined the impacts of aerosol–radiation interactions and aerosol dynamics on volcanic aerosol dispersion. They showed that during the first days after the Raikoke eruption, the absorption of solar radiation caused by the presence of ash had a significant impact on the aerosol dispersion, producing a self-lofting effect on the plume. Over the course of 4 d after the eruption, the maximum cloud top height rose more than 6 km (Muser et al., 2020). Within a few weeks the volcanic plume dispersed across the Northern Hemisphere (NH) and was continually observed months after the eruption. The radiative self-lofting could explain some of the differences between observations and model simulations, which did not account for ash in previous studies (Haywood et al., 2010; Kloss et al., 2021) since the self-lofting effect would result in a greater fraction of the plume in the stratosphere and subsequently result in a longer residence time. Stenchikov et al. (2021) also found in model experiments of the Pinatubo eruption that during the first week after the eruption SO_2 and sulfate plumes in the presence of ash rose 7 km above injection. It has been shown that whilst the ash does not provide a direct climate impact and the aerosol optical depth decreases quickly, the impact of the ash on the dynamical lofting of the plume is very important for the mass of the aerosol remaining in the stratosphere (Stenchikov et al., 2021).

Several studies have also discussed the influence of self-lofting caused by the presence of soot from intense forest fires (e.g. Fromm et al., 2005; Peterson et al., 2018; Christian et al., 2019; Damany-Pearce, 2022). Of particular note are the studies of Ansmann et al. (2021) and Ohneiser et al. (2021), who used state-of-the-art lidar retrievals mounted on an icebreaker ship that drifted in the Arctic Circle during winter 2020 to infer that biomass burning smoke from intense Siberian wildfires was present in significant quantities in the lower stratosphere, although these results remain contentious (e.g. Boone et al., 2022). We restrict our study to simulations of the Raikoke eruption including and excluding volcanic ash.

The aim of this study is to assess the modelled volcanic emissions that best represent the observed Raikoke volcanic eruption. We compare observations with a model simulation injecting only SO_2 with a model simulation with both SO_2 and ash. We use these to establish how well UKESM1 performs in modelling the volcanic plume and to determine if the inclusion of ash in modelled volcanic emissions leads to a better agreement with observations. In Sect. 2 we introduce the observational datasets used and the differences in retrieval techniques. Furthermore, we provide a description of UKESM1 and the simulation set-up in Sect. 3. In Sect. 4 we present the results and discussion before conclusions are drawn in Sect. 5.

2 Observational data and quality assurance

2.1 CALIPSO

The Cloud-Aerosol Lidar and Infrared Pathfinder Satellite Observation (CALIPSO) satellite (Winker et al., 2009) combines an active lidar instrument with passive infrared and visible imagers to analyse the vertical structure and properties of thin cloud and aerosols. The Cloud-Aerosol Lidar with Orthogonal Polarization (CALIOP) instrument is a dual-wavelength (532 and 1064 nm) polarisation-sensitive lidar that provides high-resolution vertical profiles of aerosols and clouds. The aerosol profile products are reported at a uniform spatial resolution of 5 km horizontally. The vertical resolution of the data varies as a function of altitude, with 60 m vertical resolution in the troposphere and 180 m vertical resolution in the stratosphere.

This study uses quality-assured (QA) daily averaged vertical profiles of aerosol extinction (km^{-1}) at 532 nm from the v4.20 CALIOP 5 km level 2 Cloud and Aerosol Profile data product. Aerosol extinction coefficients are reported for each bin in which aerosol particulates were detected, those in which no aerosols were detected contain fill values (-9999) and those in which the extinction retrieval failed were assigned a fill value of -333 . These were mapped to a $1^\circ \times 1^\circ$ latitude and longitude spatial grid whilst maintaining the original vertical profile. Quality control procedures were applied to the data in a similar fashion to those implemented in Campbell et al. (2012), which includes quality assurance as to the stability of the retrievals and accounts for missing data when retrieval stability fails. The stratospheric aerosol optical depth is calculated by integrating over altitudes above the observed tropopause.

Active lidar retrievals, such as those obtained by CALIOP, are susceptible to solar background contamination, which results in poorer performance in daytime conditions, resulting in different minimum detection thresholds. It is estimated that the night-time threshold is 0.012 km^{-1} and the daytime threshold is 0.067 km^{-1} (Toth et al., 2018). The daytime detection threshold results in a column-integrated underestimate of the AOD, and it has been found that it is unable

to detect around 50 % of aerosol profiles when the AOD is less than 0.1 (Toth et al., 2018). For this reason, this study only uses the night-time retrievals to create the daily average extinction values to avoid an underestimated daily average. However, utilising only the night-time profiles leads to large areas of missing data, specifically at high latitudes during the Northern Hemisphere summer where areas experience 24 h of sunlight. At most northern latitudes (60–90° N), the CALIOP night-time profiles miss the initial peak in aerosol between 30 and 100 d after the eruption. Whilst the maximum night-time sAOD is approximately 65 % greater than the peak daytime sAOD, evaluating only the night-time profiles could influence the timing of the sAOD peak. This is discussed further in Sect. 4.

2.2 OMPS

The Suomi National Polar-orbiting Partnership (NPP) is a weather satellite that was launched in 2011 with five imaging systems, including the Ozone Mapping and Profiler Suite (OMPS), a series of instruments comprised of back-scattered ultraviolet radiation sensors. These sensors measure and monitor atmospheric trace gases, aerosols, surface reflectance, and cloud-top pressure. There is global spatial coverage providing a good opportunity to evaluate the plume at high latitudes. Retrieved profiles have a vertical resolution of approximately 1.8 km, with profiles being measured from the ground to about 80 km (Taha et al., 2021).

2.2.1 OMPS-NM

The OMPS Nadir Mapper (NM) measures backscattered UV radiance spectra between 300 and 380 nm, and whilst it is primarily designed to measure global total ozone, the SO₂ vertical column amount can be derived from the hyperspectral measurements of the OMPS-NM instrument. This study utilises the SO₂ level 2 orbital products to assess the distribution of SO₂ after the eruption. A QA scheme is applied to daily profiles of total column SO₂ data, retrieved with a prescribed lower-stratospheric profile centred at 16 km above the surface. The screening includes discarding pixels when the solar zenith angle is greater than approximately 88° or the viewing zenith angle is greater than approximately 70° (Yang, 2017).

2.2.2 OMPS-LP

In addition to the CALIOP aerosol extinction data, we utilise retrievals of the vertical aerosol extinction coefficient (km⁻¹) from the OMPS Limb Profiler (LP). The OMPS-LP is a passive sensor that looks back along the orbit track at the Earth's limb and records atmospheric spectra that are used to retrieve aerosol extinction coefficient profiles from the lower stratosphere (10–15 km) to the upper stratosphere (55 km). Aerosol extinction measurements are provided at

wavelengths ranging between 510 and 997 nm at 1 km altitude intervals between the surface and 40.5 km. This study utilises the v2.0 data measured at 869 nm, which has been found to be the best OMPS-retrieved wavelength relative to SAGE III (Taha et al., 2021). Relative to V1.5 data, an improved cloud screening criterion is used in V2.0, which does not remove fresh volcanic plumes and allows us to use the filtered retrieved extinction coefficient data product that removes the influence of polar stratospheric clouds (Taha et al., 2021). As with the CALIOP data, quality control procedures are applied to the OMPS-LP data. These include removing values where the cumulative residual error exceeds a threshold value, when the single scattering viewing angle exceeds 145°, and where the derived aerosol scattering index is less than 0.01 (Johnson et al., 2020).

Due to the viewing geometry and sensitivity of the instrument, OMPS-LP can detect aerosol extinction coefficient values down to a minimum value of $1 \times 10^{-5} \text{ km}^{-1}$ (Johnson et al., 2020), which is far more sensitive than CALIOP (Sect. 2.1.1). However, OMPS-LP experiences loss of sensitivity of short wavelength radiances to aerosols, caused by Rayleigh scattering and aerosol attenuation of the limb-scattered radiation, which is most pronounced below ~17 km and especially in the Southern Hemisphere (Johnson et al., 2020). The retrieval issues described here, particularly the altitude sensitivity, have a significant impact on our study since it was estimated that the initial plume reached altitudes of between 11 and 20 km (Vaughan et al., 2021; Osborne et al., 2022); therefore, we utilise the 869 nm wavelength data and scale the data to 532 nm to compare to CALIOP. However, once the self-lofting of the plume occurs, and it is dispersed over the Northern Hemisphere, it is expected that the increased sAOD becomes more readily detectable by OMPS-LP (Hirsch and Koren, 2021), while it becomes less detectable or undetectable by CALIOP due to CALIOP's significantly higher minimum detection threshold. This is examined in more detail in Sect. 4.

2.3 AERONET

AERONET provides whole atmosphere AOD observations at a series of sites distributed across the globe, providing a good global coverage of ground-based remote sensing data. One of these sites, the Mauna Loa Observatory (MLO), located at 3397 m above sea level in Hawaii, provides an excellent opportunity to monitor stratospheric events. The measurement site is generally removed from the influence of pollution sources and is located at an altitude higher than most tropospheric aerosols. This provides an opportunity to retrieve ground-based observations of the stratosphere using sun photometry with minimal tropospheric influences. MLO has been monitoring the stratospheric aerosol layer with lidar since 1975 (Barnes and Hofmann, 1997), providing a long-term historical record, and previous studies have demonstrated that aerosol from the Raikoke plume was readily de-

Table 1. The aerosol size distribution in GLOMAP-mode, including the aerosol modes represented, the range of radii that these include, and their geometric standard deviation.

Aerosol mode	Radii (nm)	σ_g
Nucleation sol.	0–5	1.59
Aitken sol.	5–50	1.59
Accumulation sol.	50–250	1.40
Coarse sol.	250–5000	2.00
Aitken insol.	5–50	1.59

tectable (Chouza et al., 2020). Rather than lidars, this study uses daily level 2 AOD AERONET retrievals measured at 500 nm that are automatically cleared of cloud and that have undergone quality assurance.

3 Model simulations

3.1 UKESM1

UKESM1 is the latest UK Earth system model, described by Sellar et al. (2019). UKESM1 consists of the HadGEM3 coupled physical climate model with additional interactive components including modelling key biogeochemical processes (Yool et al., 2013), tropospheric and stratospheric chemistry (Archibald et al., 2020), aerosols (Mann et al., 2010), and sea ice (Ridley et al., 2018). The atmosphere has a horizontal resolution of 1.25° latitude by 1.875° longitude with 85 vertical levels and a model top at around 85 km (Storkey et al., 2018). The StratTrop chemical mechanism used in UKESM1 is described by Archibald et al. (2020). This merged stratospheric and tropospheric scheme simulates interactive chemistry from the surface to the top of the model, including oxidation reactions responsible for sulfate aerosol production (Sellar et al., 2019).

Atmospheric composition in UKESM1 is simulated by the UK Chemistry and Aerosols (UKCA) sub-model. One of the main components of UKCA is the GLOMAP-mode modal aerosol scheme described in Mann et al. (2010) and (2012). GLOMAP-mode is a two-moment aerosol microphysics scheme that simulates speciated aerosol mass and number across five lognormal size modes, four soluble modes (nucleation, Aitken, accumulation, and coarse modes), and one insoluble Aitken mode. The prognostic aerosol species represented are sulfate, black carbon, organic carbon, and sea salt, with species within each mode treated as an internal mixture. The size ranges covered by each mode are shown in Table 1.

This configuration for UKESM1 and UKCA has been used in many studies to model the evolution of sulfur dioxide into sulfate aerosol. This was done most recently by Vioni et al. (2023) and Bednarz et al. (2023), who examined the evolution and climate impacts of the sulfur dioxide and sulfate plumes under continuous stratospheric injection in three different models. In terms of the distribution and sulfate aerosol

optical depth, the resultant plume from UKESM1 when injecting at the most northerly latitude in that study (30° N) was broadly consistent with that from both CESM2 and GISS models, lending confidence to the ability of UKESM1 to accurately model middle-to-high-latitude stratospheric injections.

In addition to the UKCA aerosol components, mineral dust is included as an externally mixed aerosol via the CLASSIC (Coupled Large-scale Aerosol Simulator for Studies In Climate) six-bin scheme detailed in Woodward (2011), which represents mineral dust with diameters ranging from approximately 0.06 to 60 μm . This scheme is modified to provide a suitable proxy for volcanic ash as detailed in Sect. 3.2.

3.2 Simulations and reference wavelengths for model and observation intercomparisons

Simulations of the Raikoke and Ulawun eruptions were performed by nudging horizontal winds towards ERA5 reanalysis data to produce relevant meteorological conditions for the respective period using the atmosphere-only configuration of UKESM1. Nudged simulations were performed without any explosive volcanic emissions as a control (CNTL), with SO₂ emissions only (SO₂only), and with SO₂ and ash emissions (SO₂ + ash). The Raikoke eruption was initiated for the 24 h period starting at 00:00 UTC on 21 June 2019 with a constant emission rate. Emissions were injected into a single column within the model framework at two injection altitudes, a lower “tropospheric” injection at 10 km, and an upper “stratospheric” injection at 13–15 km where the emissions were distributed equally across the altitude range. A total of 1.5 Tg SO₂ (Kloss et al., 2021) was injected, and for the SO₂ + ash scenario 1.1 Tg of ash (Muser et al., 2020) was also injected at the same altitudes as SO₂. Injection altitudes and masses of SO₂ and ash are consistent with observations and those found in the literature (Muser et al., 2020; Kloss et al., 2021; De Leeuw et al., 2021). The emission profile was weighted so that 80 % was emitted into the stratosphere and the remaining 20 % into the troposphere based on observations of the SO₂ vertical profile (De Leeuw et al., 2021; Osborne et al., 2022).

Emissions of ash are implemented by adapting the Woodward (2011) bin scheme for mineral dust as a suitable proxy. The justification for doing this stems from the fact that the refractive indices and size distributions are similar (e.g. Millington et al., 2012; Johnson et al., 2012; Osborne et al., 2022), although it is recognised that substantial inter-eruption and inter-eruption-phase variability in volcanic ash refractive indices occurs (e.g. Millington et al., 2012; Turnbull et al., 2012). The ash is moderately absorbing, with a refractive index of $1.52 + 0.0015i$, based on the mineral dust from Balkanski et al. (2007) with the medium level of hematite (1.5 %). Volcanic ash size distributions were based on observations of the Eyjafjallajökull eruption presented in Johnson et al. (2012) fitted by lognormal distributions (Ta-

ble 5 of Johnson et al., 2012). The lognormal parameters for the overall mean aerosol size distribution include a volume geometric mean diameter of 3.8 and standard deviation of 1.85. Transport and deposition of dust is as described in detail in Woodward (2001), with improvements to the emission scheme and refractive index data described in Woodward et al. (2022). In the current configuration mineral dust aerosol is simulated independently of other aerosol species using the CLASSIC dust scheme (Bellouin et al., 2011). Mineral dust can therefore be considered externally mixed with the GLOMAP aerosols.

For both SO₂only and SO₂ + ash simulations, the Ulawun eruptions are simulated by UKESM1 with an SO₂-only injection (no ash emissions) and are initiated on 26 June and 3 August 2019. Injection altitudes for Ulawun were 13–17 km (26 June) and 14–17 km (3 August) using 0.14 and 0.30 Tg SO₂, respectively (Kloss et al., 2021).

To facilitate the intercomparison of the observations and the model simulations all datasets were scaled to 532 nm. Mie scattering calculations were performed using the Mie scattering code within SOCRATES (Suite Of Community RAdiative Transfer codes based on Edwards and Slingo; Edwards and Slingo, 1996) to generate the single-scattering properties of volcanic aerosol at a range of specified wavelengths. Note that both the Mie scattering code and SOCRATES are used in the radiative transfer code within UKESM1. The size distribution of the volcanic aerosol used here was based upon the bimodal lognormal size distribution for a moderate loading volcanic eruption (Thomason and Peter, 2006). Specific extinction coefficients were calculated to allow all observational and model data to be scaled to one consistent wavelength: 532 nm.

4 Results

In analysing the results, we examine the injection of the SO₂ and ash through to the gas-phase oxidation of the SO₂ to sulfate aerosol and the ultimate deposition of the aerosol until the stratospheric perturbation is no longer detectable. Different aspects are investigated, including the geographic distribution and temporal evolution of the SO₂ and sulfate aerosol and the latitudinal distribution and vertical profile of the sulfate aerosol.

4.1 Observed and modelled SO₂ including and excluding volcanic ash

Figure 1 shows the evolution of the SO₂ cloud from 22 June through to the 30 June 2019. The middle column shows the OMPS-NM observations, with the UKESM1 SO₂only and SO₂ + ash simulations on the left and the right, respectively. We see that the position and timing of the plume is relatively well modelled throughout this period in both simulations. There is little difference in the spatial pattern of the SO₂ plume in both simulations, making it difficult to de-

termine based upon SO₂ alone which simulation best represents the observations. Qualitatively, the spatial pattern of the plume is better represented in both the model simulations from 26 June onwards, with both the easterly and westerly parts of the plume being well modelled. The largest difference between the observations and the model simulations is seen on 22 June where the model is initially much more diffuse. This is due to the eruption taking place at 18:00 UTC on 21 June, and it was inherently explosive and sporadic in nature compared to the smooth injection rates that are assumed in the model. This could explain why the modelled plume does not represent the observations that well during the first 2 d after the eruption. Similar conclusions have been found in a recent modelling study that uses the CALIOP lidar to assess the fidelity of an operational dispersion model in determining the evolution of a large pyrocumulonimbus event (Osborne et al., 2022; their Fig. 7). Since the model does a reasonable job at representing the shape and distribution of the plume after a few days and our objectives are to assess the general model performance over a period of many months, we retain our simplified emission period and assumed vertical profile. Higher-resolution modelling assessments using the Met Office Numerical Atmospheric-dispersion Modelling Environment (NAME) that are more appropriate for operational monitoring of volcanic plumes for the first few weeks after the eruption for the purposes of aviation safety are available in de Leeuw et al. (2021) and Osborne et al. (2022).

In the first few days after the eruption the SO₂ plume becomes trapped within a cyclonic circulation across eastern Russia and Alaska (e.g. Osborne et al., 2022). We can observe this feature in both the observations and the model simulations. However, as observed in other similar studies of other volcanic eruptions (e.g. Haywood et al., 2010) the model SO₂ plume becomes more diffuse than observations over time. We can see that as the plume evolves, despite the model capturing the general position, the model overestimates the tail crossing North America and underestimates the magnitude of the plume over Russia. This could also be due to the instrumental detection limits, where the plume has become so diffuse it becomes undetectable. We also notice that the model is generally more diffuse than the observations, which has been observed with other numerical transport schemes (e.g. de Leeuw et al., 2021) and could contribute to the differences seen in the modelled and observed tails.

To provide a more quantitative analysis of the geographic evolution we employ a dichotomous forecast style analysis. A contingency table is a simple way to identify the frequency of “yes, an event will happen” and “no, the event will not happen” forecasts and occurrences. For this analysis we treat the model simulation as the forecast and the observations as the occurrence for each grid box on each day. There are four combinations of simulations and observations, “hits” – the model simulates the observations correctly, “model > observations” – the model overestimates the obser-

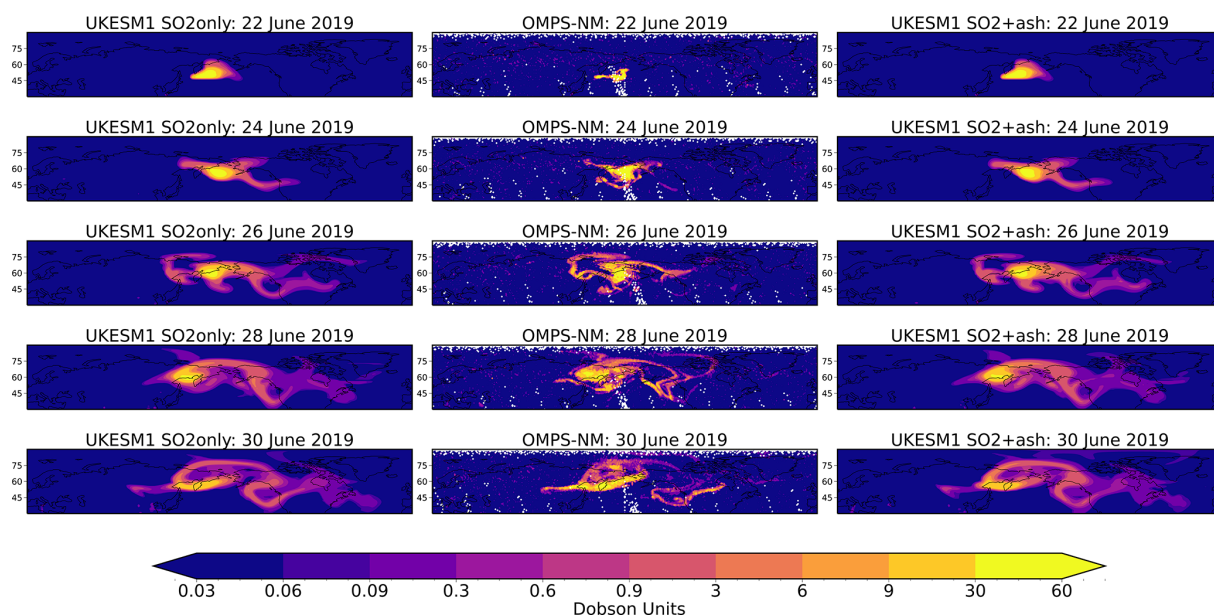


Figure 1. Geographic evolution of column-integrated SO₂ plume in Dobson units (DU) derived from the OMPS-NM lower-stratospheric profile (centre), UKESM1 SO₂only (left), and SO₂ + ash (right) for the period 22–30 June 2019. We remove the long-term background SO₂ burden derived from OMPS-NM for the years 2013–2018 from those for 2019 to provide a stratospheric perturbation for the observations. Similarly, we remove the impacts of background stratospheric aerosol from the model simulations by subtracting the stratospheric sulfate burdens from the CNTL simulation from those for SO₂only and SO₂ + ash. The OMPS-LP background and CNTL SO₂ burden are shown in Fig. S1.

vations, “observations > model” – the model underestimates the observations and “correct negative” – both the observations and the model are below a given threshold, 0.3 Dobson units (DU). In developing the contingency table we consider estimates of error, such as timing errors in synoptic meteorological features that frequently occur in weather forecasting, and the fact that the model and observations are not perfectly co-located in time. We therefore assume that the observations are uncertain by a factor of 2 and use these as the upper and lower bounds. However, we recognise that much more detailed and comprehensive approaches to forecast verification have been developed (e.g. Casati et al., 2008).

Figure 2 presents this analysis for the first 10 d after the eruption. Both simulations show a similar distribution, so we focus on SO₂only here. It is clear that model > observations dominates, with a large tail over North America, as seen in Fig. 1. However there are some regions where the model is underestimating the observations that may not have been identified by eye in Fig. 1. Over the 20 d after the eruption, approximately the time for the oxidation of SO₂ to sulfate aerosol, both model simulations overestimate the observed plume 52 % of the time. We also note that between 15 % and 17 % of the plume is correctly modelled within the bounds of the observations for both simulations, with SO₂ + ash underestimating the observations 3 % more than SO₂only (Table 2).

In Fig. 1 we can see that the SO₂ plume travels longitudinally and moves towards more northern latitudes, as we would expect from the stratospheric Brewer–Dobson circulation (e.g. Haynes, 2005) and as evidenced from the previous eruption of Sarychev Peak (Haywood et al., 2010; Jégou et al., 2013). Due to this poleward transport, it is unlikely that the Raikoke SO₂ plume would travel south of 30° N, particularly in the first few months after the eruption. Hence, to avoid any influence from the Ulawun eruption, we take the area-weighted average from 30–90° N (discussed further in Sect. 4.3) to determine the temporal evolution of SO₂ and calculate an *e*-folding time. Figure 3 shows the daily column burden of observed and modelled SO₂ after the eruption. The spike seen at approximately day 60 is an artefact from the long-term background SO₂ burden. The observations show a peak column burden of 0.76 DU and have an *e*-folding time of 20 d. Model simulations had similar *e*-folding times of 19 and 21 d for SO₂only and SO₂ + ash, respectively. This suggests that the oxidation processes are well represented in the UKESM1 model and are very similar to those determined for the Sarychev Peak eruption for the fore-running HadGEM-2 climate model (Haywood et al., 2010). However, in both SO₂only and SO₂ + ash model simulations the peak SO₂ column burden is only 0.44 DU, considerably less than that observed by OMPS-NM. The notable difference between the observations and the model is unexpected given that the magnitude of SO₂ injected was based on ob-

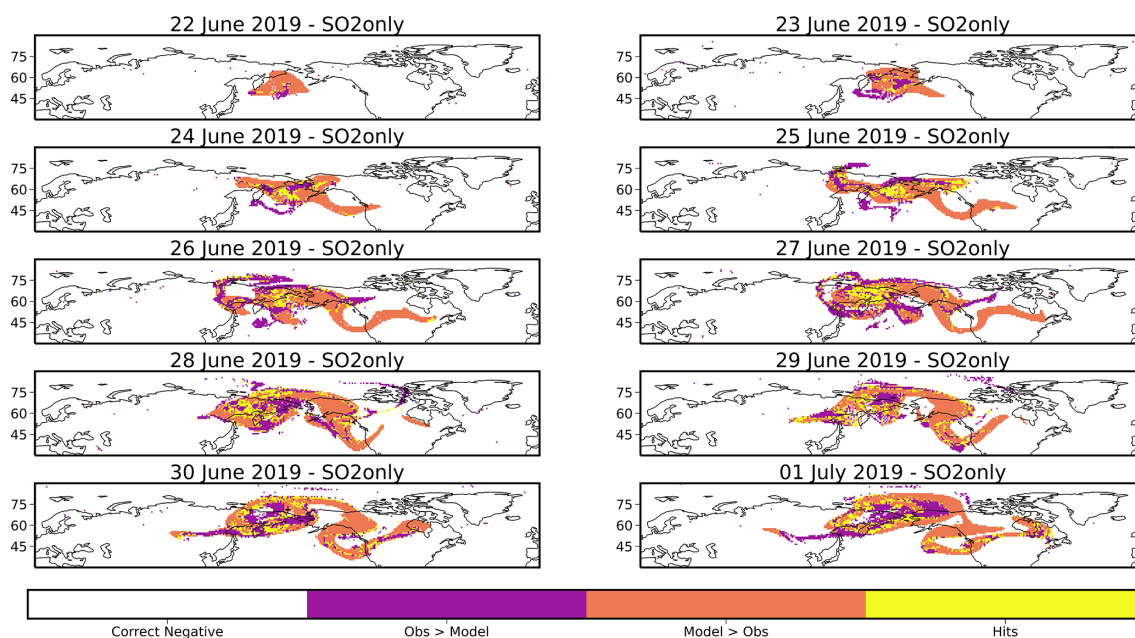


Figure 2. Contingency analysis of SO₂ plume between the OMPS-NM lower-stratospheric profile and UKESM1 SO₂only for the period 22 June–1 July 2019. “Correct negative” occurs at the point where both the model and observation are below 0.3 DU. “Hits” occur at the point where the modelled column SO₂ burden is within a factor of 2 of the observations at that point to allow for timing errors. “Obs > model” and “model > obs” occur when the modelled column SO₂ burden is above or below the factor of 2 limit.

Table 2. Contingency analysis of SO₂ plume between the OMPS-NM lower-stratospheric profile and UKESM1 SO₂only and SO₂ + ash for the 20 d following the eruption on 21 June 2019. “Hits” occur at the point where the modelled column SO₂ burden is within a factor of 2 of the observations at that point to allow for timing errors. “Obs > model” and “model > obs” occur when the modelled column SO₂ burden is above or below the factor of 2 limit.

	Hits	Observations > model	Model > observations
SO ₂ only	17 %	31 %	52 %
SO ₂ + ash	15 %	34 %	51 %

servations (Muser et al., 2020; Kloss et al., 2021; De Leeuw et al., 2021). However, if the amount of SO₂ injected into the model simulations were to be increased it would lead to a significant overestimate of sulfate aerosol and sAOD (see Sects. 4.2, 4.4, and 4.6). For this reason we do not change the amount of SO₂ injected. We do note that the 1.5 Tg of SO₂ that we chose to inject into UKESM1 is based upon measurements from TROPOMI and HIMAWARI data and therefore may not exactly correlate with the OMPS-NM data.

4.2 Distribution of sulfate aerosol

To investigate the distribution and evolution of the sulfate plume we utilise the CALIOP and OMPS-LP retrieved aerosol extinction integrated above the tropopause to find the perturbed sAOD. We firstly investigate the temporal evolution of the zonal mean sAOD by performing similar analysis to previous studies (e.g. Kravitz et al., 2010; Haywood et al., 2010; Kloss et al., 2021). We compare the evolution of

the OMPS-LP and CALIOP retrievals against the UKESM1 SO₂only and SO₂ + ash scenarios, shown in Fig. 4. Due to the differences in satellite retrievals discussed in Sect. 2, there are seasonal gaps in the data from as far south as $\sim 55^\circ$ N in CALIOP night-time retrievals, due to polar summer and $\sim 65^\circ$ N in OMPS-LP due to the lack of daylight hours in NH winter. Additionally, the observations have different minimum retrieval limits (0.012 km^{-1} for CALIOP, $1 \times 10^{-5} \text{ km}^{-1}$ for OMPS-LP), and thus to ensure better comparisons we have applied both requirements to both model simulations and scaled all data to a wavelength of 532 nm. The CALIOP retrieval only reports the aerosol extinction coefficient for layers in which aerosol particulates were detected above the minimum retrieval limit and uses fill values for the rest of the profile. Therefore, it is important to note that the CALIOP sAOD could be biased towards large values of aerosol extinction during the first few months after the eruption and towards smaller values after the plume has become more diffuse.

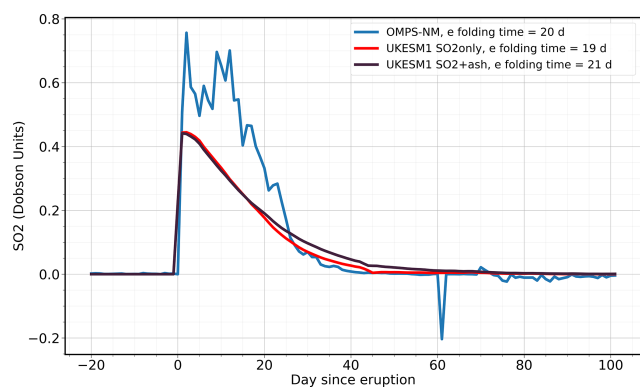


Figure 3. Daily perturbation of SO_2 in Dobson units (DU) derived from the OMPS-NM lower-stratospheric profile (blue), UKESM1 SO_2 only (red), and SO_2 + ash (dark purple). Data are averaged across latitudes $30\text{--}90^\circ\text{N}$ and weighted by the cosine of the corresponding latitude to ensure the data are area weighted. We remove the long-term background SO_2 burden derived from OMPS-NM for the years 2013–2018 from those for 2019 to provide a stratospheric perturbation for the observations. Similarly, we remove the impacts of background stratospheric aerosol from the model simulations by subtracting the stratospheric sulfate burdens from the CNTL simulation from those for SO_2 only and SO_2 + ash.

Figure 4c shows the evolution of zonal mean sAOD derived from OMPS-LP from June 2019 to May 2020. The zonal peak sAOD occurs ~ 1.5 months after the eruption, which is similar to the findings in Gorkavyi et al. (2021). The impact on the sAOD in OMPS-LP is still present 1 year later, with values of sAOD not yet returned to their pre-eruption values. This contrasts with Fig. 4d, the same quantity derived from CALIOP, where the perturbation of sAOD is significantly reduced by December 2019, and by March and April 2020 zonal sAOD values are similar to those found pre-eruption. We can confidently attribute this difference in aerosol lifetime to the high aerosol extinction minimum detection threshold for aerosol extinction associated with the CALIOP dataset. Figure 4b and f display the UKESM1 SO_2 only and SO_2 + ash zonal mean sAOD with the CALIOP minimum retrieval limits applied where a similar distribution to that seen in the observations is modelled, indicating that the shorter aerosol lifetime observed in the CALIOP retrievals compared to OMPS-LP is due to high detection limits. As the plume disperses over time, the plume becomes more diffuse and becomes undetectable by CALIOP, leading to under-detection, and hence the integrated sAOD reduces much more rapidly than we see in the OMPS-LP data, which does not have the same high minimum detection threshold.

In both sets of observations (Fig. 4c and d) we can see that the enhanced stratospheric aerosol layer has been transported poleward by the Brewer–Dobson circulation with the highest sAODs found north of the eruption. The model simulations represent this transport relatively well with similar distribu-

tions to both OMPS-LP and CALIOP observations. However, in all cases the peak magnitude is overestimated, especially in the SO_2 + ash case. Whilst the peak sAOD in the SO_2 only simulation (Fig. 4a and b) is less of an overestimate of the observations compared to SO_2 + ash, it does not reproduce the evolution of the plume as well as the SO_2 + ash simulation (Fig. 4e and f) in either case. Despite the SO_2 + ash simulation (Fig. 4f) representing the CALIOP retrievals well, it is not representative of how the plume evolves over time after becoming too diffuse for CALIOP detection limits. However, as OMPS-LP has a much lower minimum detection threshold, as a dedicated stratospheric limb-profiler the decay rate of sAOD is much slower. We see a similar decay rate in the SO_2 + ash simulation (Fig. 4e) with comparable magnitudes to the OMPS-LP observations from December onwards. From Fig. 4 we can begin to infer that the SO_2 + ash simulation represents the evolution of zonal sAOD better than the SO_2 only case, but this inference is far from conclusive. Further comparisons to the model are made in Sect. 4.4.

4.3 Temporal evolution of sulfate aerosol

The CALIOP- and OMPS-LP-derived perturbations of sAOD from the long-term mean are presented in Fig. 5. As seen in Fig. 4, the two satellite observations have different temporal evolutions. Comparing the early stages of the plume evolution it is clear that OMPS-LP does not detect the same high peak in sAOD as CALIOP; however, as previously mentioned, the mean CALIOP sAOD could be biased towards higher values of aerosol extinction due to fill values below the minimum retrieval limit. The CALIOP dataset shows a clear peak 60 d after the eruption with an sAOD of approximately 0.026, whereas OMPS-LP reaches a peak sAOD of approximately 0.015 over 3 months after the eruption. Studies have suggested that limb instruments such as OMPS-LP can fail to detect aerosol near the tropopause (e.g. Fromm et al., 2014). However, since CALIOP is a nadir-viewing lidar the altitude of the plume does not significantly affect the retrieval. This could contribute to the difference we see in the initial sAOD peaks since the plume was detected at altitudes as low as 11 km (Hedelt et al., 2019; Vaughan et al., 2021). The vertical profile of the plume is explored further in Sect. 4.6. We also see a big difference in the decay rate of sAOD. The CALIOP observations have an e -folding time of 84 d, in contrast to OMPS-LP, which has an e -folding time of 220 d. As previously discussed, the difference in decay rate between CALIOP and OMPS-LP is likely due to the different minimum detection thresholds for both satellites. Once the plume begins to dilute and become more diffuse the higher CALIOP detection threshold (0.012 km^{-1}) results in under-detection in comparison to OMPS-LP, which has a much lower threshold ($1 \times 10^{-5}\text{ km}^{-1}$) and is thus able to detect more of the diffuse plume.

We have created a combined dataset that includes aerosol extinction data from both CALIOP and OMPS-LP, as seen

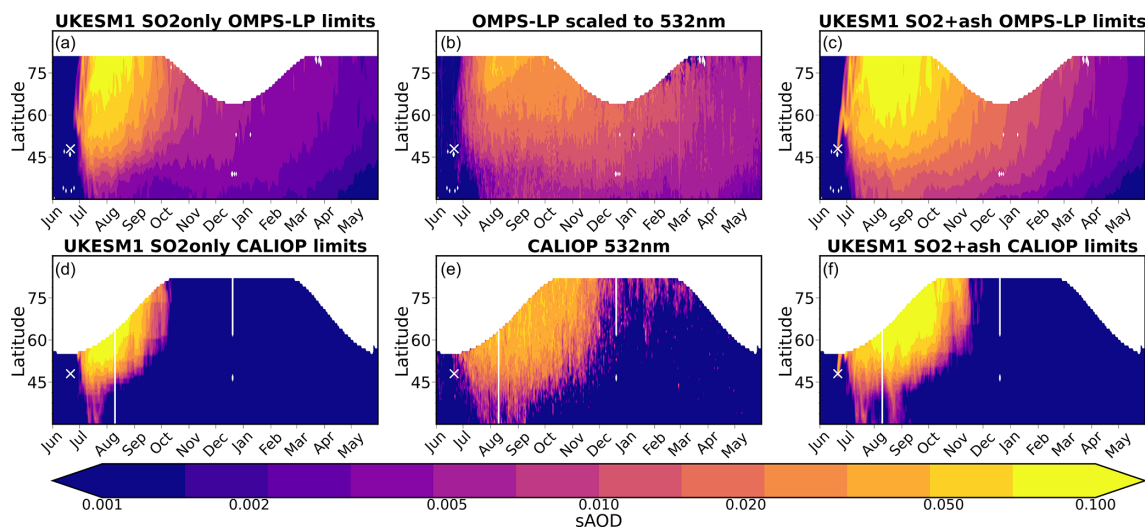


Figure 4. Latitude–time distribution of the zonally averaged sAOD from 30 to 90° N. **(a)** UKESM1 SO₂only masked for OMPS-LP observations, scaled from 550 to 532 nm; **(b)** OMPS-LP observations scaled from 869 to 532 nm; **(c)** UKESM1 SO₂ + ash masked for OMPS-LP observations, scaled from 550 to 532 nm; **(d)** UKESM1 SO₂only masked for CALIOP observations, with sAOD calculated with values of aerosol extinction < 0.012 km⁻¹ and the CALIOP minimum detection limit scaled to 532 nm; **(e)** CALIOP observations at 532 nm; and **(f)** UKESM1 SO₂ + ash masked for CALIOP observations, with sAOD calculated with values of aerosol extinction < 0.012 km⁻¹ and the CALIOP minimum detection limit scaled to 532 nm. The location of Raikoke is marked with a white cross.

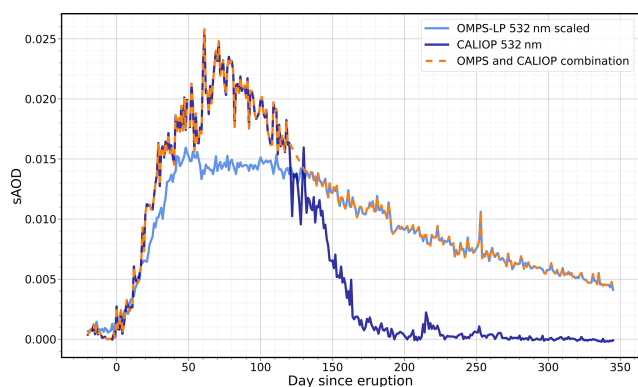


Figure 5. Daily perturbation in the sAOD averaged over 30–90° N as observed by OMPS-LP scaled from 510 to 532 nm (light blue) and CALIOP at 532 nm (dark blue). The dashed orange line represents the combined OMPS-LP and CALIOP dataset at 532 nm. We remove the long-term background sAOD derived from OMPS-LP (0.0041) and CALIOP (0.0003) for the years 2013–2018 from those for 2019 to provide a stratospheric perturbation for the observations.

in Fig. 5. The combined dataset utilises the area-averaged (30–90° N) CALIOP sAOD data for the first 4 months after the eruption before it is linearly interpolated over the region in which the two datasets cross over and then employs OMPS-LP data for the remaining months. This new dataset has an *e*-folding time of 145 d, and we believe that it is more physically reasonable than using a single observational dataset due to the data constraints outlined above. To

confirm qualitatively that using the OMPS-LP data is more appropriate than CALIOP in the later months after the eruption we use in situ ground-based data to provide an alternative comparison to these satellite datasets. We utilise the AERONET level 2 AOD retrievals measured at 550 nm and scale them to 532 nm for comparison with the satellite observations. To calculate the satellite retrievals at MLO, an area average is taken across multiple grid boxes encompassing the MLO. Note that AERONET retrievals of sAOD are not a point measurement as they are a function of the solar zenith angle. For solar zenith angles of 60–80° and assuming that any aerosol is located in the lowest 20 km above the observatory, aerosol within a 35–115 km radius of the Mauna Loa observatory is included in the observations. The same area is used to calculate the average monthly SO₂only and SO₂ + ash perturbations.

Average monthly perturbations from the long-term mean (or control simulation) for the Mauna Loa observatory are presented in Table 3. The AERONET retrievals are statistically significant at the 5% level from the long-term mean from September to November and increase to a peak AOD of 12.12×10^{-3} in September, over 2 months after the eruption. The OMPS-LP retrievals and SO₂ + ash model show a similar pattern with peak AODs in September of 7.07×10^{-3} (OMPS-LP) and 8.46×10^{-3} (SO₂ + ash). The SO₂only simulation follows a similar pattern of increased AOD between August and November; however, the magnitude of AOD is much smaller than the AERONET and OMPS-LP observations. OMPS-LP retrievals are also significantly greater than the long-term mean from August until

Table 3. Perturbation of AOD from the long-term mean retrieved from the Mauna Loa Observatory AERONET site scaled to 532 nm. OMPS-LP, UKESM1 SO₂only, and SO₂ + ash sAOD perturbation calculated across an area encompassing the MLO (19–20° N, 152–156° W). Observations highlighted with bold text are statistically significantly greater than the long-term mean at 95 % confidence level. Negative values of AOD are a result of calculating the perturbation from the long-term mean (2013–2018).

	AERONET	OMPS-LP	UKESM1 SO ₂ only	UKESM1 SO ₂ + ash
August	5.89×10^{-3}	2.16×10^{-3}	2.78×10^{-3}	4.27×10^{-3}
September	12.12×10^{-3}	7.07×10^{-3}	3.03×10^{-3}	8.46×10^{-3}
October	9.78×10^{-3}	6.41×10^{-3}	3.33×10^{-3}	7.12×10^{-3}
November	4.70×10^{-3}	4.89×10^{-3}	2.91×10^{-3}	5.40×10^{-3}
December	1.05×10^{-3}	3.81×10^{-3}	2.12×10^{-3}	3.96×10^{-3}
Average	6.71×10^{-3}	4.87×10^{-3}	2.83×10^{-3}	5.84×10^{-3}

December. CALIOP, however, does not appear to detect any statistically significant perturbation to the sAOD, with values an order of 10^2 smaller than those observed by AERONET and OMPS-LP. This is most likely due to aerosol loadings falling below the minimum detection threshold and the plume becoming more diffuse at this latitude. We also calculate the model average perturbed AOD for this region from August to December, presented in Table 3. The SO₂ + ash average AOD, 5.84×10^{-3} , agrees well with the AERONET and OMPS-LP observations of 6.71×10^{-3} and 4.87×10^{-3} , respectively. However, the SO₂only average AOD is much smaller, suggesting that the SO₂ + ash simulation validates better against this specific set of observations.

MLO is located at 19.5° N, around 30° S of Raikoke. Due to its proximity to the 5° S Ulawun eruption, there is the potential for this eruption to influence observational data. Model simulations were run without Ulawun emissions (discussed further in Sect. 4.7), and a negligible influence on the AOD in the MLO region over this time period was observed. While there may indeed be an influence from Ulawun on the AODs determined at Mauna Loa in the observational record, this modelling and the observed timing of the statistically significant AOD perturbations suggest that any influence is small. As we noted in Fig. 4, most of the aerosol plume travelled poleward via the Brewer–Dobson circulation; however, there was some southern transport seen in both satellite observations in late July and August. We can observe this further in Fig. 6 through the monthly average sAOD observed by OMPS-LP and CALIOP.

A similar analysis performed by Haywood et al. (2010) for the Sarychev eruption reveals 550 nm AOD perturbations of +0.010 and +0.008 for July and August. Given that the Sarychev and Raikoke eruptions occurred within a few calendar days of each other but in different years, it appears that the equatorward transport of aerosol for the Sarychev eruption was quicker than for the Raikoke eruption. This conclusion holds despite any potential influence from the eruption of Ulawun and highlights that considerable differences in transport can occur for volcanic eruptions that are ostensibly

very similar in terms of latitude, timing, injection amount, and vertical distribution (Jones et al., 2016).

Figure 6 shows the monthly geographic evolution of the sAOD in the Northern Hemisphere. MLO is highlighted on the first plot by a red cross. From this plot we can see that transport to lower latitudes does not occur until August; however, the CALIOP retrievals are much more diffuse than those observed in OMPS-LP. We observe high values of sAOD at high latitudes with peaks across Greenland and northern Canada. Despite the missing data in the CALIOP observations we can still see a reasonable spatial agreement in the sAOD during the first few months. In October an interesting feature is seen in the OMPS-LP data where a band of enhanced sAOD is observed between 0–15° N. This might be attributed to the second Ulawun (5.05° S, 151° E) eruption on 3 August which, owing to the latitude and altitude of the eruption, is likely to be confined by the so-called “tropical pipe” between approximately 15° S–15° N (e.g. Plumb, 1996), although some leakage to higher latitudes might be expected over time. From August onwards the stratospheric aerosol layer south of the Equator has been shown to become enhanced. Kloss et al. (2021) estimate that the aerosol from the Ulawun eruption circled the Earth in the tropics within 1 month. During October and November the sAOD in the tropical stratosphere becomes increasingly enhanced, which is likely due to the influence of Ulawun. Due to the influence of Ulawun this study uses area averages from 30 to 90° N to ensure analysis focuses solely on the impact of the Raikoke eruption. Despite the potential influence of Ulawun on MLO observations, we can nevertheless conclude that combining the initial CALIOP peak and the latter half of the OMPS-LP data is the most appropriate representation of the plume evolution since OMPS-LP does not observe the initial peak, whereas CALIOP detection limits lead to non-detection of aerosol once it has become diffuse, and hence it apparently reduces the observed lifetime and *e*-folding time of the sulfate aerosol.

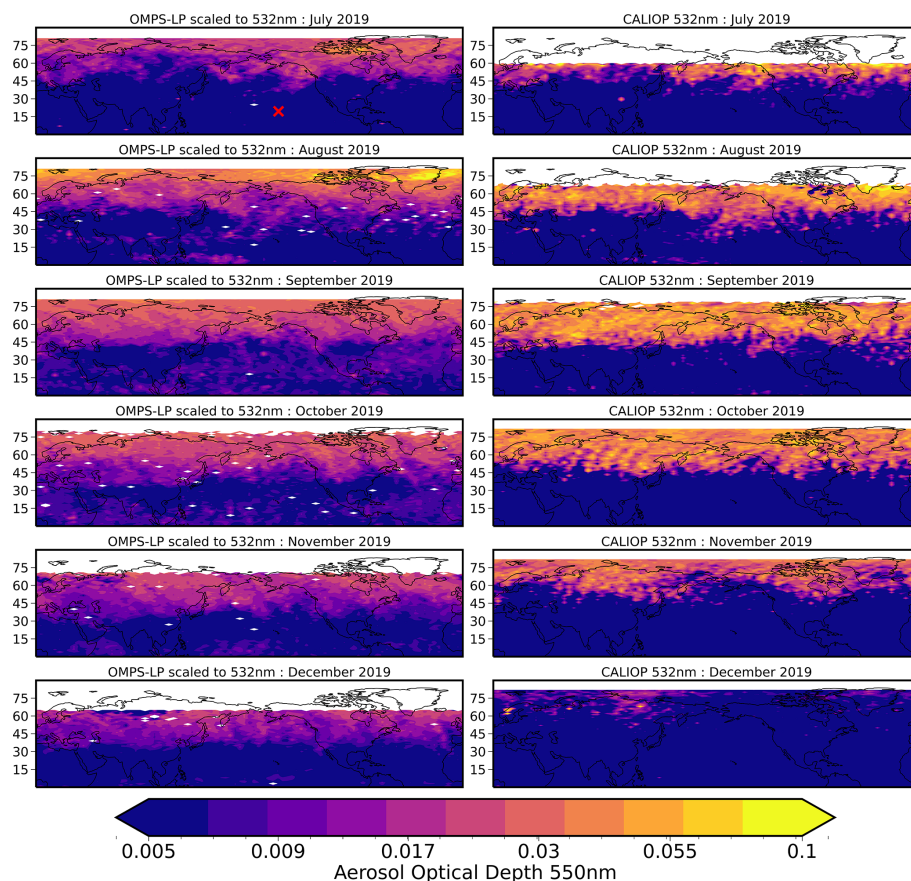


Figure 6. Monthly geographic evolution of the Northern Hemisphere sAOD from July 2019 to December 2019 derived from OMPS-LP retrieved aerosol extinction (left) and CALIOP aerosol extinction profile (right). We remove the long-term background sAOD derived from OMPS-LP and CALIOP for the years 2013–2018 from those for 2019 to provide a stratospheric perturbation for the observations.

4.4 Model comparison

To make consistent and accurate comparisons between the combined satellite dataset and the model simulations it is appropriate to implement the same method used in Fig. 4 and apply minimum detection and spatial limits to the model data. Figure 7 compares the combined OMPS-LP and CALIOP dataset to the two model simulations both with (solid lines) and without (dashed lines) the respective observational limits applied. For the first 4 months after the eruption the combined dataset uses the CALIOP observations; therefore, we use the CALIOP minimum detection threshold (0.012 km^{-1}) to filter out aerosol extinction values in the model simulations before calculating the sAOD for comparison. After this we apply the limits of the OMPS-LP data to the model simulations in a similar fashion since OMPS-LP is used in the combined observational dataset for the following months. For both SO₂only and SO₂ + ash we only include model data where observational data were available. When the observational limits were applied, no linear interpolation across the location where the combined dataset switches from CALIOP to OMPS-LP was applied to the model simu-

lations owing to the considerable difference in sAOD across the area of interpolation.

Figure 7 clearly demonstrates significant differences between the sulfate aerosol evolution in the SO₂only and SO₂ + ash simulations. Considering first the SO₂only simulations, we note that the timing of the peak is much earlier in SO₂only compared to the observations. The combined observational dataset peaks at approximately 0.026 around 2 months after the eruption and has an *e*-folding time of 145 d. For the SO₂only simulations, when including the observational limits, which is considered the most appropriate method of comparison, the peak sAOD is much greater (0.033) and earlier than observations. We observe a similarly fast decrease in sAOD when observational limits are applied to SO₂only (*e*-folding time of 45 d), whereby the sAOD drops to values close to zero at day 110 before an increase at approximately day 125 after the eruption. This abrupt change is an artefact of combining CALIOP and OMPS-LP limits in the SO₂only simulation to best compare against the combined observational dataset.

Now we consider the SO₂ + ash simulations. In contrast to the SO₂only simulation, there is a large difference in the

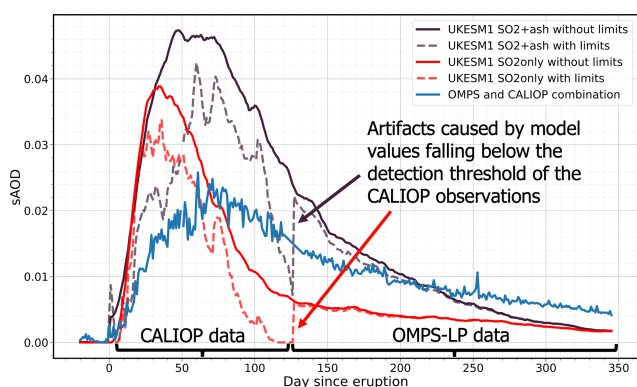


Figure 7. Daily perturbation of sAOD at 532 nm averaged over 30–90° N. Daily OMPS-LP and CALIOP combined dataset sAOD (blue), UKESM1 SO₂only with observational limits applied (red) and without limits applied (dashed red), and UKESM1 SO₂ + ash with observational limits applied (dark purple) and without limits applied (dashed dark purple). We remove the long-term background sAOD derived from OMPS-LP and CALIOP for the years 2013–2018 from those for 2019 to provide a stratospheric perturbation for the observations. Similarly, we remove the impacts of background stratospheric aerosol from the model simulations by subtracting the sAOD from the CNTL simulation from those for SO₂only and SO₂ + ash.

first 50 d after the eruption between the SO₂ + ash model with and without limits. When observational limits are applied (as is recommended), the peak sAOD (0.042), whilst still an overestimate, occurs 60 d after the eruption, which is more consistent with the combined observational dataset. The delay in the peak of sAOD when observational limits are applied can be attributed in part to the missing data at high latitudes during the polar summer since we can still identify this delay in the peak sAOD when we only apply spatial CALIOP limits to SO₂ + ash. We can see in Figs. 4 and 6 that the sulfate aerosol travels poleward due to the Brewer–Dobson circulation, and we would expect the resulting sAOD to be greatest within the first few months after the eruption. However, since the months following the eruption are the Northern Hemisphere summer, there are no CALIOP night retrievals at high latitudes, contributing to the appearance of a delayed sAOD peak.

When observational limits are applied to SO₂ + ash we observe a decline in model sAOD after the peak owing to transfer from the stratosphere to the troposphere with an *e*-folding time of 90 d, almost 2 months faster than the observed data. The initial steep decline in SO₂ + ash is due to the CALIOP limits imposed upon the model. At approximately day 135 after the eruption there is a sharp increase in modelled sAOD. This is an artefact of combining SO₂ + ash with CALIOP limits and SO₂ + ash with OMPS-LP limits. The SO₂ + ash simulation with CALIOP limits applied has a much faster decay rate with an *e*-folding time of 44 d, whereas the SO₂ + ash simulation with OMPS-LP limits has

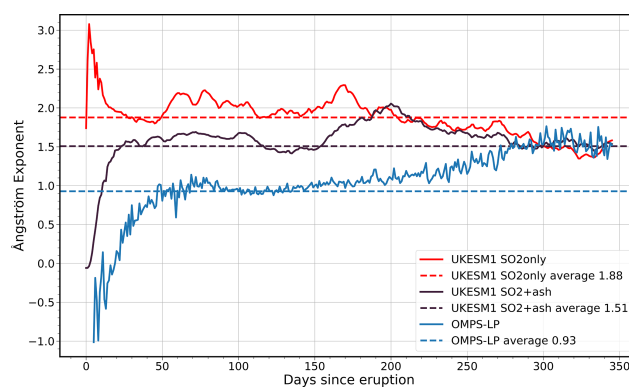


Figure 8. Daily evolution of the Ångström exponent for OMPS-LP (blue), UKESM1 SO₂only (red), and UKESM1 SO₂ + ash (dark purple) calculated using area-weighted sAOD between 30 and 90° N (same as Fig. 7) using 510 and 869 nm wavelengths.

a much longer *e*-folding time of 101 d. Whilst SO₂ + ash is not perfect at recreating the sAOD evolution, we can see that by applying the observational limits it starts to become apparent that SO₂ + ash provides a better comparison against observations than SO₂only, although some considerable differences still exist. In the following two sections we explore changes to the stratospheric aerosol Ångström exponent and the vertical profile evolution of the aerosol to further examine the consistency of the SO₂only and SO₂ + ash simulations against observations.

4.5 Analysis of stratospheric aerosol Ångström exponents

Without detailed in situ measurements (e.g. Jégou et al., 2013) it is not possible to know the detailed size distribution of the volcanic aerosols with a high level of accuracy. However, the wavelength dependence can be used to calculate the Ångström exponent (AE), since it is often used as an indicator of aerosol particle size. For measurements of optical depth τ , and at wavelengths λ_1 , λ_2 , the AE is given by Eq. (1):

$$\alpha = -\log \frac{\tau_{\lambda_1}}{\tau_{\lambda_2}} / \log \frac{\lambda_1}{\lambda_2}. \quad (1)$$

The OMPS-LP aerosol extinction measurements are provided at wavelengths ranging between 510–997 nm, presenting the opportunity to calculate the sAOD and analyse the evolution of the AE and consequently variations in the aerosol size distribution after the eruption. Figure 8 shows the daily AE for OMPS-LP, SO₂only, and SO₂ + ash calculated using the area-averaged sAOD at wavelengths of 510 and 869 nm between 30 and 90° N.

The observations show that the AE is initially close to between -1 and 0 , indicating that large particles were observed immediately after the eruption, and it therefore contains a significant amount of volcanic ash. After around 50 d after

the eruption, the AE increases to approximately 1 for a period of over 3 months, this could suggest that the largest particles had dropped out and smaller particles remained. As the time after the eruption increases, the AE increases to a maximum value of ~ 1.6 . Kloss et al. (2021) estimate a pristine average AE of 1.7 using background sAODs, which suggests that approximately 300 d after the eruption the observations have returned to pre-eruption AE average.

Both model simulations converge on an AE of around 1.6 after 300 d; however, they both display starkly contrasting behaviour immediately after the eruption. In the SO₂only scenario the initial AE is very high (up to around 3), indicating smaller particles and decreases with time. The behaviour of the AE is therefore the opposite of what is observed.

In comparison, during the first 10 d after the eruption, the SO₂ + ash scenario initially shows an AE of around zero due to the presence of ash, which then increases as the ash falls out from the atmosphere. This behaviour is much more similar to what we see in the observations as compared to SO₂only, confirming that our SO₂ + ash simulations are in better agreement with observations. However, the agreement is far from perfect, with the model AE increasing much faster than what we see in the observations, it then converges with the SO₂only scenario approximately 200 d after the eruption. Considering an internal mixture between ash and sulfate in the model could potentially resolve the differences between the observations and the model AE. However, the slower increase in the observed AE could also indicate an influence from pumice or soot particles from forest fires. Despite these differences, this figure again suggests that the SO₂ + ash scenario is better at representing the observations compared to the SO₂only case. Further discussion of this is provided in Sect. 5.

4.6 Aerosol extinction vertical profile analysis

Figure 9 shows the vertical evolution of the CALIOP-derived aerosol extinction coefficient with monthly averages and standard deviation from July until December. We also include both model simulations, SO₂only (dashed red line) and SO₂ + ash (solid red line), for comparison. The observed monthly tropopause height (mean and standard deviation) is also included to highlight tropospheric and stratospheric altitudes. Both observations and model simulations are averaged over 30–90° N, not including those latitudes where CALIOP night retrievals are unable to retrieve data due to polar summer. Since CALIOP aerosol extinction retrievals have a minimum detection threshold of 0.012 km^{-1} (Toth et al., 2018), this limit has also been applied to the SO₂only and SO₂ + ash data for a more consistent comparison.

In the CALIOP observations we can see that initially after the eruption there are two peaks at ~ 11 and ~ 14.5 km, similar to the two injection altitudes used to initialise the UKESM1 simulations. The observations then form a singular peak above the average tropopause at ~ 14 km, which in-

creases in magnitude to a peak of $5.3 \times 10^{-3} \text{ km}^{-1}$ between September and October. In comparison, the two model simulations peak at $8.3 \times 10^{-3} \text{ km}^{-1}$ for SO₂only at ~ 12 km and $9.1 \times 10^{-3} \text{ km}^{-1}$ for SO₂ + ash at ~ 13.5 km. We notice a considerable difference in the altitude of the plume between the two model simulations. In July the peak aerosol extinction for SO₂only is at approximately 13 km, a similar altitude to the average tropopause height. In contrast to this, the SO₂ + ash plume has a peak aerosol extinction at ~ 15 km. This initial difference in height results in a significant impact on the lifetime of the aerosol. To explore the impact of the altitude of the plume further, we look at Fig. 10, which displays the aerosol extinction coefficient as a function of latitude and altitude. This avoids averaging over a widely varying tropopause height and allows us to examine the altitude of the plume in the models and observations against the altitude of the tropopause and how it might affect the aerosol lifetime.

As per the analysis shown in Fig. 9, we impose the CALIOP detection limits onto the model simulations and only include latitudes in which CALIOP data is available. The average monthly tropopause height is included and shown by the black line. The initial difference between the plume altitude of SO₂only and SO₂ + ash is striking. Already in July we observe some aerosol in the midlatitudes below the monthly tropopause height, with a substantial portion below the tropopause in August. However, we do not see this in the SO₂ + ash model until September and October. The CALIOP observations reveal the poleward transport of the aerosol via the Brewer–Dobson circulation from July through until September. This is reproduced reasonably well in the SO₂ + ash model; however, we do not observe this in the SO₂only simulation. Similarly, the magnitude and spatial distribution of the aerosol in October is well modelled by SO₂ + ash compared to SO₂only in which only a negligible aerosol extinction coefficient is found.

Due to more removal processes in the troposphere, the altitude of the plume in relation to the tropopause height can impact the decay rate and lifetime of the aerosol. Since both model scenarios were initialised with the same SO₂ injection altitudes, the difference between plume altitudes in July must be due to the self-lofting effect from the ash. Muser et al. (2020) had documented this for the Raikoke plume and noted that the maximum cloud-top height rose more than 6 km within the first few days after the eruption. Whilst the SO₂ + ash scenario overestimates the magnitude of the aerosol extinction coefficient in the first few months, it does represent the altitude and lifetime of the aerosol plume well. The impact of the self-lofting effect is also seen in Fig. S2, which displays the stratospheric aerosol optical depth of SO₂ + ash and SO₂only, alongside the sAOD derived from the CLASSIC dust emission and SO₂ + ash minus the sAOD from dust. We can see here that the impact from the ash itself is relatively negligible, and therefore it must be the impact

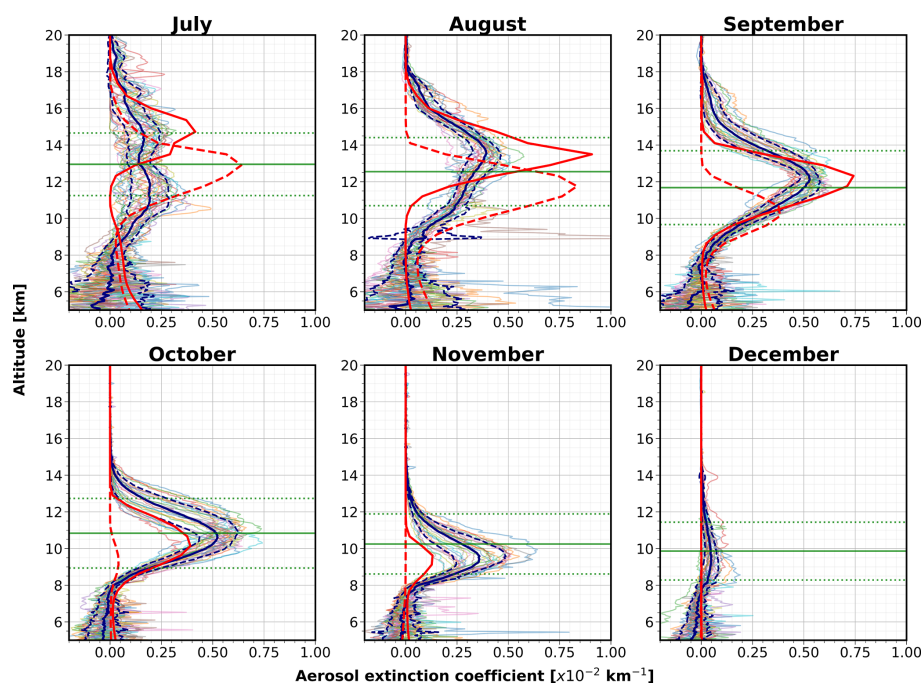


Figure 9. Aerosol extinction coefficient vertical profile averaged longitudinally and over 30–90° N. Averaged daily CALIOP aerosol extinction coefficient vertical profiles (night retrievals only, fainter lines) with monthly average (bold blue) and monthly average plus or minus standard deviation (solid dashed black lines). UKESM1 SO₂ + ash (solid bold red) and SO₂only (dashed bold red) simulations with imposed CALIOP minimum retrieval limits and masks. Average tropopause height is shown by the horizontal green line and the average tropopause height ± 1 standard deviation for 2019 is also shown as dotted green lines.

the ash has on the sulfate aerosol that drives the changes seen in sAOD.

The vertical profile analysis of the CALIOP aerosol extinction coefficient indicates how close the volcanic plume was to the tropopause in the first month or so after the eruption. This could explain why the OMPS-LP dataset missed the initial sAOD peak as limb instruments can fail to detect aerosol near the tropopause (e.g. Fromm et al., 2014). Analysis of the aerosol size evolution and vertical profile in the model simulations have confirmed that the UKESM1 SO₂ + ash simulation is more consistent with the observations. Figures 8, 9, and 10 illustrate that SO₂ + ash provides a much better representation of the aerosol size and lifetime and therefore resulting climatic impact than the SO₂only scenario.

4.7 Radiative forcing

Haywood et al. (2010) ran simulations of the Sarychev eruption over a 3-month period in June–August 2009 and explored the difference between the aerosol optical depth and radiative forcing due to anthropogenic aerosol and the Sarychev Peak stratospheric aerosol plume. They found that in some regions of the NH the AOD was of comparable magnitude or greater than the AOD from anthropogenic emissions. We estimate the impact of the Raikoke eruption on

the approximate radiative forcing exerted by the volcanic aerosol and compare this to the Sarychev Peak eruption. In Fig. 11 we have recreated the Sarychev Peak AOD and radiative forcing plots from Haywood et al. (2010, their Fig. 12) using data from HadGEM2 and compare them against our UKESM1 Raikoke simulations, eliminating the impacts of the Ulawun eruption. As in the results presented by Haywood et al. (2010), our UKESM1 simulations are nudged to reanalysis data, but the evolutions of the control and experiment simulations differ slightly and result in some differences in the cloud and fields. Due to this, the all-sky radiative forcing cannot be accurately determined from the difference in the top of the atmosphere shortwave upwelling radiation with and without aerosols. The all-sky shortwave radiative forcing can be approximated for purely scattering aerosol, following the calculation used by Haywood et al. (2010), using the following equation:

$$\text{Radiative forcing} \approx (\text{SW}_{\text{CTL}} - \text{SW}_{\text{EXP}}) \times (1 - A_c), \quad (2)$$

where SW is the clear-sky outgoing shortwave radiation (W m^{-2}) at the top of the atmosphere (TOA) for the control (CTL) and experiment (EXP) and A_c is the cloud fraction (Haywood et al., 1997). This assumes that the contributions from longwave radiation and the radiative forcing from cloudy areas are negligible. It has been shown through radiative transfer calculations that this is a reasonable assumption

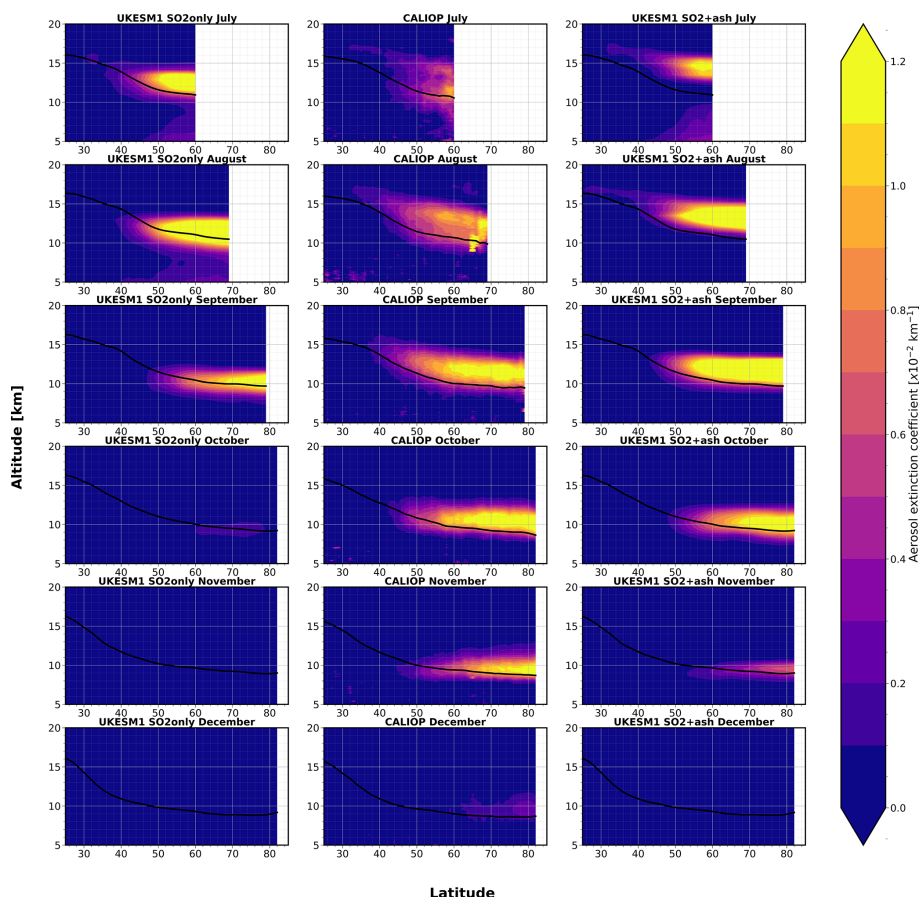


Figure 10. Aerosol extinction coefficient vertical profile averaged longitudinally. Averaged monthly CALIOP (centre) aerosol extinction coefficient vertical profiles (night retrievals only) with monthly average tropopause height (solid black). UKESM1 SO₂only (left) and SO₂ + ash (right) simulations with imposed CALIOP minimum retrieval limits and masks.

for conservative scattering from sulfate aerosols for optically thick cloud (e.g. Haywood and Shine, 1997).

Figure 11 shows the months in which the different eruptions peak in both AOD and radiative forcing. In order to make global comparisons between the Sarychev Peak eruption and Raikoke, we perform a UKESM1 simulation in which we do not include the Ulawun eruption. We see in both plots that the Raikoke eruption had a greater impact on the global AOD and resulted in a larger cloud-free radiative forcing at its peak. After the Sarychev Peak eruption, the NH average AOD peaked in July at approximately 0.01, this is in comparison to Raikoke, where the peak NH-averaged AOD occurred in August at approximately 0.03. The global and NH radiative forcing impacts from both eruptions from June through until August are shown in Table 4.

Rather counter-intuitively, the cloud-free radiative forcing is some 20 % stronger for the SO₂only simulations than for the SO₂ + ash simulations. The explanation for this result is that, as in the case for clouds, the evolution of the aerosol differs slightly between the SO₂only and the SO₂ + ash simulations. This results in sAODs that are some 20 % larger

over areas of central Eurasia in July and August, which are predominantly cloud-free areas in the model at that time of year. This results in cloud-free radiative forcings that are a factor of 1.2 greater for the SO₂only simulations than the SO₂ + ash simulations. However, far greater fractional differences of up to a factor of 3.5 are evident in subsequent months owing to the general reduction in the sAOD documented in previous sections.

While the cloud-free radiative forcing from June cannot be directly compared owing to differences in timing of the eruptions (Sarychev eruption initiated on 15 June in Haywood et al., 2010, but 21 June in this study), the global mean cloud-free radiative forcing from the Raikoke eruption in comparison to the Sarychev Peak eruption are substantially greater in July and August. At their peaks, the NH cloud-free radiative forcing of Raikoke is -0.48 W m^{-2} , almost twice as strong as that of Sarychev Peak (-0.24 W m^{-2}). This is due to a combination of factors including (but not limited to) (i) the base-state model (UKESM1 versus HadGEM2); (ii) the aerosol modelling scheme (UKCA versus CLASSIC); (iii) differences in assumed vertical emission profile (80 % at

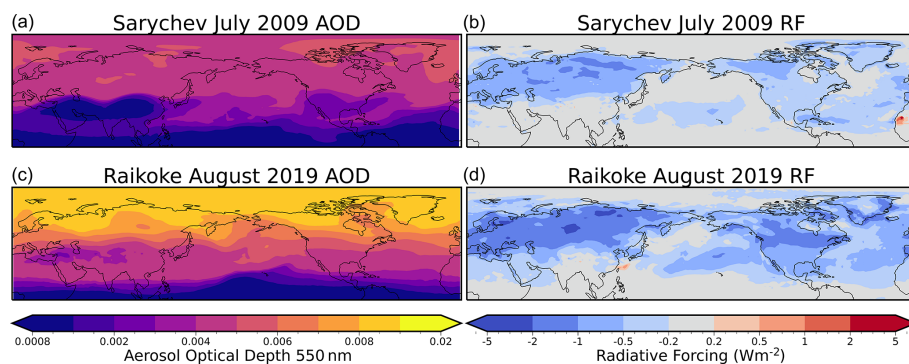


Figure 11. The sAOD for July at 550 nm for (a) Sarychev Peak derived from HadGEM2 and (b) Raikoke derived from UKESM1. The cloud-free radiative forcing at the top of the atmosphere (W m^{-2}) for (c) Sarychev Peak derived from HadGEM2 and (d) Raikoke derived from UKESM1.

Table 4. The cloud-free global mean radiative forcing (in W m^{-2}) at the top of the atmosphere for Sarychev Peak (after Haywood et al., 2010) derived from HadGEM2 and for Raikoke SO_2 only and SO_2 + ash simulations derived from UKESM1. N/A indicates not available.

	Raikoke SO_2 only	Raikoke SO_2 + ash	Sarychev Peak
June	−0.001	−0.004	−0.03
July	−0.26	−0.22	−0.13
August	−0.29	−0.25	−0.07
September	−0.13	−0.19	N/A
October	−0.05	−0.14	N/A
November	−0.02	−0.07	N/A

13–15 km versus evenly distributed between 11–15 km); and (iv) differing meteorological conditions, which have been shown to significantly impact aerosol distribution, lifetime, and radiative forcing, particularly for emissions close to the tropopause (Jones et al., 2016). Note that the inclusion of volcanic ash does not appear to be a significant cause of the increased peak radiative forcing compared to the Sarychev analysis; the inclusion of ash appears to have a greater impact on the longevity of the radiative forcing through enhanced stratospheric aerosol lifetime. To fully evaluate differences across model formulations would require re-runs of the model for the Sarychev case with UKESM1, which is beyond the scope of this study.

5 Summary and conclusion

This study provides an analysis of satellite and ground-based observational data to determine if including ash in model simulations of volcanic eruptions can more accurately represent aerosol size, geographic distribution, and the evolution of volcanic plumes. There are substantial differences between observations due to different observational limitations. Whilst these were difficult to reconcile, we were able to apply numerous observational thresholds to UKESM1 to assess the ability of the model to replicate observations. Using multiple remote sensing methods we were able to validate the trans-

port of the SO_2 plume and the evolution of the sulfate aerosol and associated radiative impacts modelled by the UKESM1 nudged to ERA5 reanalysis data.

The Raikoke eruption was the largest volcanic injection of SO_2 into the stratosphere since the OMPS satellite was launched and was well observed by OMPS-NM and OMPS-LP. This revealed that the plume became trapped within a cyclonic circulation for several days across eastern Russia and Alaska before travelling eastwards across North America and the North Atlantic. This agrees with other satellite observations used in previous studies (e.g. Kloss et al., 2021; Vaughan et al., 2021). When nudged to ERA5 reanalysis data the UKESM1 SO_2 only and SO_2 + ash simulations were able to represent the position of the main features of the plume evolution, including the cyclonic circulation. Similarly to other models (e.g. Haywood et al., 2010; de Leeuw et al., 2021) the model simulations produce a more diffuse SO_2 plume compared to observations due to a combination of model uncertainty and observational limits.

The distribution of the sulfate aerosol plume was examined using two satellite observations with comparisons to the UKESM1 model simulations. The zonal evolution observed by CALIOP and OMPS-LP followed a similar geographic evolution to the Sarychev Peak eruption in June 2009 (Haywood et al., 2010), which was to be expected since they are neighbouring volcanoes and the altitude and injection mag-

nitude of Sarychev Peak (11–15 km, 1.2 ± 0.2 Tg) were similar to that of Raikoke (10–15 km, 1.5 ± 0.2 Tg). Due to differences in minimum detection thresholds it was observed that the CALIOP data did not represent the long-term evolution of the sulfate aerosol plume well, and similarly to other limb instruments OMPS-LP can fail to detect aerosol near the tropopause at the beginning of an eruption. Hence, we created a combined dataset consisting of both CALIOP and OMPS-LP aerosol extinction data. Data from the Mauna Loa Observatory provided additional corroborative evidence that the OMPS-LP observations were more appropriate after the plume had dispersed, with CALIOP observations showing no significant increase in sAOD for the eruption year. Model simulations differed in the MLO region, with the SO₂ + ash case presenting similar values of sAOD to both the OMPS-LP and AERONET observations. In contrast, the SO₂only simulation revealed values of sAOD much lower than those seen in the observations and SO₂ + ash case.

We then studied the observed Ångström exponent utilising the OMPS-LP 869 and 510 nm wavelength aerosol extinction coefficient retrievals. Throughout the first 50 d after the eruption the AE was less than 1, indicating the presence of large aerosol particles. Comparing the observations to both the SO₂only and SO₂ + ash UKESM1 scenarios demonstrates that whilst both models do not capture the observations completely, the SO₂ + ash scenario better represents the change in aerosol size after the eruption. It is also an indicator that the model removes the ash much faster than we see in the observations. Zhu et al. (2020) proposed that after the 2014 Mount Kelud eruption the volcanic aerosol layer was primarily composed of low-density, super-micrometre-sized ash. Most model simulations assume volcanic ash particles are denser than the pumice-like particles observed in Zhu et al. (2020) and hence the ash particles in model simulations fall out more quickly. Figure S2 highlights the relatively small and short impact the ash in the model has on the stratospheric aerosol optical depth itself. Instead we see in Figs. 9 and 10 how the ash produces a self-lofting effect onto the sulfate aerosol, extending the stratospheric lifetime of the aerosol. This could explain the difference between the observations and the SO₂ + ash model case. Obviously, there are limitations to our assumption that the ash is externally mixed with the sulfate aerosol, as in reality there will be varying degrees of internal and external mixture.

It is possible that the observations were also influenced by the Canadian and Siberian wildfires that occurred in the summer of 2019. A few days before the Raikoke eruption (17 June 2019), wildfires in Alberta, Canada, produced biomass burning aerosols and formed pyrocumulus clouds that entered the lower stratosphere. By late June the resulting aerosol layers arrived over the UK and Europe; this was only a few days before aerosols originating from the Raikoke plume were observed by UK lidar (Osborne et al., 2022). The Siberian wildfires were extreme and lasted from 19 July to 14 August 2019 (between 28–54 d after the eruption; Johnson

et al., 2021), injecting wildfire smoke into the troposphere near the Arctic region. Ohneiser et al. (2021) and Ansmann et al. (2021) suggested that the influence from the Siberian wildfire smoke increased the aerosol optical depth across the Arctic region. However, this finding is challenged by Boone et al. (2022). Whilst there might have been some influence on the aerosol optical properties and distribution from these events, our simulations suggest that the SO₂ + ash model provides a reasonable representation of the Raikoke eruption without including the Siberian wildfires in the model simulation. Our work certainly shows that using the results from a single climate model simulation of Sarychev to infer aerosol optical depths for other volcanic eruptions such as Raikoke is inadvisable. Further work appears necessary to elucidate whether biomass burning smoke aerosols play a role in the elevated aerosol concentrations in the polar vortex during the Northern Hemisphere winter of 2020.

We utilised the CALIOP aerosol extinction coefficient night-time retrievals to examine the evolution of the vertical profile of the plume. We initially observed two distinct peaks just above and just below the average tropopause height before a singular peak at around 14 km was observed from August onwards. The SO₂ + ash model represents the altitude of the aerosol well throughout the months following the eruption; however, the SO₂only simulation displayed values of aerosol extinction consistently lower in altitude (Figs. 9 and 10), resulting in a much faster decay rate due to transfer to the troposphere through tropospheric folds. The modelled aerosol extinction peak was prematurely early and overestimated in both scenarios which could be due to the rate of coagulation in the stratosphere or how the model represents new particle formation. After more moderate volcanic eruptions the rate of coagulation can be slower, resulting in smaller less optically active particles and a delayed aerosol extinction peak. We see in both model simulations that the accumulation mode dominates the column aerosol burden. This could suggest that the rate of transfer from the optically inactive Aitken mode to the optically active accumulation mode in the model may be too fast.

Finally, the impact of the modelled Raikoke eruption was compared to the HadGEM2 simulation of the Sarychev Peak eruption. The Northern Hemisphere peak mean perturbation to the sAOD after the Sarychev Peak eruption was 0.01 (compared to 0.03 after the Raikoke eruption). The greatest radiative forcing on the Northern Hemisphere after the Raikoke eruption was 0.48 W m^{-2} , almost double that seen in July following the Sarychev Peak eruption (0.24 W m^{-2}), despite only a 25 % increase in the injected SO₂ amount. Whilst the eruptions were similar in altitude and latitude, the impact seen in UKESM1 is far greater for Raikoke than after Sarychev Peak. Some of these differences may stem from the large dependence on meteorology that has been noted for low-altitude eruptions (Jones et al., 2016), with differences in how the SO₂ was injected into the model contributing to this change. We also compare an SO₂only Raikoke-

only simulation and find a Northern Hemispheric peak AOD of approximately 0.02 but a greater peak radiative forcing of 0.55 W m^{-2} . This is to be expected since the injected ash would contribute a positive radiative forcing, counterbalancing the negative radiative forcing from the sulfate aerosol. Finally, UKESM1 represents a major advance from HadGEM2 with a new core physical model including a well-resolved stratosphere and enhanced tropospheric–stratospheric chemistry.

Accurately modelling the evolution of volcanic plumes and therefore identifying the impacts they have on the climate is a difficult task. Our analysis provides several lines of evidence to suggest that including ash in model emission schemes can improve the representation of volcanic plumes in global climate models. Whilst the model is not perfect at representing each process, it provides reasonable *e*-folding times for the conversion of SO_2 to sulfate aerosol and models the geographic distribution of the aerosol well. Future work might consider internal mixture of sulfate and ash aerosol, which could yield differences in the aerosol microphysical and optical properties. Including smoke aerosol in simulations of this eruption would also be useful to identify if this would improve the model performance. A better representation of volcanic ash could also be applied because this study used mineral dust as a proxy since the refractive indices and size distributions are similar. Ultimately, this study has shown that volcanic emissions are far more complicated than simple injections of SO_2 and that limitations in remote sensing observations hamper definitive attribution of particle composition. These results suggest the strong need for in situ sampling of aerosol from instrumentation on airborne observational platforms. While such measurements of ash–sulfate mixtures have been performed following eruptions that predominantly loaded the troposphere (e.g. Johnson et al., 2021; Turnbull et al., 2012; Newman et al., 2012), the dearth of such measurements in the stratosphere means that definitive attribution of aerosol composition and microphysical and optical properties remains extremely challenging.

The final caveats to our modelling study include the fact that we do not include any emission of water vapour (e.g. Joshi and Jones, 2009) or any halogens (e.g. Staunton-Sykes et al., 2021); these species are commonly co-emitted with volcanic eruptions and may influence the oxidation rates of sulfur dioxide and the detailed evolution of the resultant aerosol plume.

Code and data availability. The data are available at <https://doi.org/10.5281/zenodo.7602563> (Wells et al., 2023), and the code to reproduce the figures is at <https://doi.org/10.5281/zenodo.7603038> (Wells, 2023).

Supplement. The supplement related to this article is available online at: <https://doi.org/10.5194/acp-23-3985-2023-supplement>.

Author contributions. AFW, MO, and LDP analysed the satellite and in situ data and created the combined observational dataset. AJ and JMH devised the experimental set-up for UKESM1. AFW, AJ, and JMH analysed the results of the simulations. AFW prepared the manuscript with contributions from all co-authors.

Competing interests. The contact author has declared that none of the authors has any competing interests.

Disclaimer. Publisher's note: Copernicus Publications remains neutral with regard to jurisdictional claims in published maps and institutional affiliations.

Acknowledgements. Alice F. Wells was funded via a UKRI Centre for Doctoral Training in Environmental Intelligence PhD studentship hosted by the University of Exeter. James M. Haywood, Andy Jones, and Martin Osborne were supported by the Met Office Hadley Centre Climate Programme funded by BEIS. James M. Haywood would like to acknowledge support from the NERC-funded EXTEND project (NE/W003880/1) and from SilverLining through its Safe Climate Research Initiative. Lilly Damany-Pearce was supported from the NERC-funded SASSO standard grant (NE/S00212X/1). James M. Haywood and Daniel G. Partridge would like to acknowledge the support of the NERC-funded ADVANCE project (NE/T006897/1).

Financial support. This research has been supported by the Natural Environment Research Council (grant no. NE/W003880/1); the Natural Environment Research Council (grant no. NE/S00212X/1); the Department for Business, Energy and Industrial Strategy, UK Government (Met Office Hadley Centre Climate Programme); the Natural Environment Research Council (grant no. NE/T006897/1); and the Centre for Doctoral Training in Environmental Intelligence: Data Science & AI for Sustainable Futures (grant no. EP/S022074/1).

Review statement. This paper was edited by Kostas Tsigaridis and reviewed by three anonymous referees.

References

- Abdelkader, M., Stenchikov, G., Pozzer, A., Tost, H., and Lelieveld, J.: The effect of ash, water vapor, and heterogeneous chemistry on the evolution of a Pinatubo-size volcanic cloud, *Atmos. Chem. Phys.*, 23, 471–500, <https://doi.org/10.5194/acp-23-471-2023>, 2023.
- Ansmann, A., Ohneiser, K., Mamouri, R.-E., Knopf, D. A., Veselovskii, I., Baars, H., Engelmann, R., Foth, A., Jimenez, C., Seifert, P., and Barja, B.: Tropospheric and stratospheric wildfire smoke profiling with lidar: mass, surface area, CCN, and INP retrieval, *Atmos. Chem. Phys.*, 21, 9779–9807, <https://doi.org/10.5194/acp-21-9779-2021>, 2021.

- Archibald, A. T., O'Connor, F. M., Abraham, N. L., Archer-Nicholls, S., Chipperfield, M. P., Dalvi, M., Folberth, G. A., Denison, F., Dhomse, S. S., Griffiths, P. T., Hardacre, C., Hewitt, A. J., Hill, R. S., Johnson, C. E., Keeble, J., Köhler, M. O., Morgenstern, O., Mulcahy, J. P., Ordóñez, C., Pope, R. J., Rumbold, S. T., Russo, M. R., Savage, N. H., Sellar, A., Stringer, M., Turnock, S. T., Wild, O., and Zeng, G.: Description and evaluation of the UKCA stratosphere–troposphere chemistry scheme (Strat-Trop v1.0) implemented in UKESM1, *Geosci. Model Dev.*, 13, 1223–1266, <https://doi.org/10.5194/gmd-13-1223-2020>, 2020.
- Balkanski, Y., Schulz, M., Claquin, T., and Guibert, S.: Reevaluation of Mineral aerosol radiative forcings suggests a better agreement with satellite and AERONET data, *Atmos. Chem. Phys.*, 7, 81–95, <https://doi.org/10.5194/acp-7-81-2007>, 2007.
- Barnes, J. E. and Hofmann, D. J.: Lidar measurements of stratospheric aerosol over Mauna Loa Observatory, *Geophys. Res. Lett.*, 24, 1923–1926, <https://doi.org/10.1029/97gl01943>, 1997.
- Bednarz, E. M., Visioni, D., Kravitz, B., Jones, A., Haywood, J. M., Richter, J., MacMartin, D. G., and Braesicke, P.: Climate response to off-equatorial stratospheric sulfur injections in three Earth system models – Part 2: Stratospheric and free-tropospheric response, *Atmos. Chem. Phys.*, 23, 687–709, <https://doi.org/10.5194/acp-23-687-2023>, 2023.
- Bellouin, N., Rae, J., Jones, A., Johnson, C., Haywood, J., and Boucher, O.: Aerosol forcing in the Climate Model Intercomparison Project (CMIP5) simulations by HadGEM2-ES and the role of ammonium nitrate, *J. Geophys. Res.-Atmos.*, 116, D20206, <https://doi.org/10.1029/2011JD016074>, 2011.
- Bluth, G. J. S., Doiron, S. D., Schnetzler, C. C., Krueger, A. J., and Walter, L. S.: Global Tracking of the SO₂ Clouds from the June 1991 Mount Pinatubo Eruptions, *Geophys. Res. Lett.*, 19, 151–154, 1992.
- Boone, C. D., Bernath, P. F., Labelle, K., and Crouse, J.: Stratospheric Aerosol Composition Observed by the Atmospheric Chemistry Experiment Following the 2019 Raikoke Eruption, *J. Geophys. Res.-Atmos.*, 127, e2022JD036600, <https://doi.org/10.1029/2022JD036600>, 2022.
- Bruckert, J., Hoshyaripour, G. A., Horváth, Á., Muser, L. O., Prata, F. J., Hoose, C., and Vogel, B.: Online treatment of eruption dynamics improves the volcanic ash and SO₂ dispersion forecast: case of the 2019 Raikoke eruption, *Atmos. Chem. Phys.*, 22, 3535–3552, <https://doi.org/10.5194/acp-22-3535-2022>, 2022.
- Cai, Z., Griessbach, S., and Hoffmann, L.: Improved estimation of volcanic SO₂ injections from satellite retrievals and Lagrangian transport simulations: the 2019 Raikoke eruption, *Atmos. Chem. Phys.*, 22, 6787–6809, <https://doi.org/10.5194/acp-22-6787-2022>, 2022.
- Campbell, J. R., Tackett, J. L., Reid, J. S., Zhang, J., Curtis, C. A., Hyer, E. J., Sessions, W. R., Westphal, D. L., Prospero, J. M., Welton, E. J., Omar, A. H., Vaughan, M. A., and Winker, D. M.: Evaluating nighttime CALIOP 0.532 μm aerosol optical depth and extinction coefficient retrievals, *Atmos. Meas. Tech.*, 5, 2143–2160, <https://doi.org/10.5194/amt-5-2143-2012>, 2012.
- Casati, B., Wilson, L. J., Stephenson, D. B., Nurmi, P., Ghelli, A., Pocerlich, M., Damrath, U., Ebert, E. E., Brown, B. G., and Mason, S.: Forecast verification: current status and future directions, *Meteorol. Appl.*, 15, 3–18, <https://doi.org/10.1002/met.52>, 2008.
- Chouza, F., Leblanc, T., Barnes, J., Brewer, M., Wang, P., and Koon, D.: Long-term (1999–2019) variability of stratospheric aerosol over Mauna Loa, Hawaii, as seen by two co-located lidars and satellite measurements, *Atmos. Chem. Phys.*, 20, 6821–6839, <https://doi.org/10.5194/acp-20-6821-2020>, 2020.
- Christian, K., Wang, J., Ge, C., Peterson, D., Hyer, E., Yorks, J., and McGill, M.: Radiative Forcing and Stratospheric Warming of Pyrocumulonimbus Smoke Aerosols: First Modeling Results With Multisensor (EPIC, CALIPSO, and CATS) Views from Space, *Geophys. Res. Lett.*, 46, 10061–10071, <https://doi.org/10.1029/2019GL082360>, 2019.
- Clarisse, L., Hurtmans, D., Clerbaux, C., Hadji-Lazaro, J., Ngadi, Y., and Coheur, P.-F.: Retrieval of sulphur dioxide from the infrared atmospheric sounding interferometer (IASI), *Atmos. Meas. Tech.*, 5, 581–594, <https://doi.org/10.5194/amt-5-581-2012>, 2012.
- Corradini, S., Merucci, L., Prata, A. J., and Piscini, A.: Volcanic ash and SO₂ in the 2008 Kasatochi eruption: Retrievals comparison from different IR satellite sensors, *J. Geophys. Res.-Atmos.*, 115, D00L21, <https://doi.org/10.1029/2009JD013634>, 2010.
- Damany-Pearce, L., Johnson, B., Wells, A., Osborne, M., Allan, J., Belcher, C., Jones, A., and Haywood, J.: Australian wildfires cause the largest stratospheric warming since Pinatubo and extends the lifetime of the Antarctic ozone hole, *Scientific Reports*, 12, 12665, <https://doi.org/10.1038/s41598-022-15794-3>, 2022.
- de Leeuw, J., Schmidt, A., Witham, C. S., Theys, N., Taylor, I. A., Grainger, R. G., Pope, R. J., Haywood, J., Osborne, M., and Kristiansen, N. I.: The 2019 Raikoke volcanic eruption – Part 1: Dispersion model simulations and satellite retrievals of volcanic sulfur dioxide, *Atmos. Chem. Phys.*, 21, 10851–10879, <https://doi.org/10.5194/acp-21-10851-2021>, 2021.
- Dhomse, S. S., Emmerson, K. M., Mann, G. W., Bellouin, N., Carslaw, K. S., Chipperfield, M. P., Hommel, R., Abraham, N. L., Telford, P., Braesicke, P., Dalvi, M., Johnson, C. E., O'Connor, F., Morgenstern, O., Pyle, J. A., Deshler, T., Zawodny, J. M., and Thomason, L. W.: Aerosol microphysics simulations of the Mt. Pinatubo eruption with the UM-UKCA composition-climate model, *Atmos. Chem. Phys.*, 14, 11221–11246, <https://doi.org/10.5194/acp-14-11221-2014>, 2014.
- Edwards, J. and Slingo, A.: Studies with a flexible new radiation code. I: Choosing a configuration for a large-scale model, *Q. J. Roy. Meteor. Soc.*, 122, 689–719, 1996.
- Fromm, M., Bevilacqua, R., Servranckx, R., Rosen, J., Thayer, J. P., Herman, J., and Larko, D.: Pyro-cumulonimbus injection of smoke to the stratosphere: Observations and impact of a super blowup in northwestern Canada on 3–4 August 1998, *J. Geophys. Res.-Atmos.*, 110, D08205, <https://doi.org/10.1029/2004JD005350>, 2005.
- Fromm, M., Kablick, G., Nedoluha, G., Carboni, E., Grainger, R., Campbell, J., and Lewis, J.: Correcting the record of volcanic stratospheric aerosol impact: Nabro and Sarychev Peak, *J. Geophys. Res.-Atmos.*, 119, 10343–10364, <https://doi.org/10.1002/2014jd021507>, 2014.
- Gordeev, E. I. and Girina, O. A.: Volcanoes and their hazard to aviation, *Herald of the Russian Academy of Sciences*, 84, 1–8, <https://doi.org/10.1134/s1019331614010079>, 2014.
- Gorkavyy, N., Krotkov, N., Li, C., Lait, L., Colarco, P., Carn, S., DeLand, M., Newman, P., Schoeberl, M., Taha, G., Torres, O., Vasilkov, A., and Joiner, J.: Tracking aerosols and SO₂ clouds from the Raikoke eruption: 3D view from

- satellite observations, *Atmos. Meas. Tech.*, 14, 7545–7563, <https://doi.org/10.5194/amt-14-7545-2021>, 2021.
- Guo, S., Bluth, G. J. S., Rose, W. I., Watson, I. M., and Prata, A. J.: Re-evaluation of SO₂ release of the 15 June 1991 Pinatubo eruption using ultraviolet and infrared satellite sensors, *Geochem. Geophys. Geosy.*, 5, Q04001, <https://doi.org/10.1029/2003gc000654>, 2004.
- Haynes, P.: Stratospheric Dynamics, *Annu. Rev. Fluid Mech.*, 37, 263–293, <https://doi.org/10.1146/annurev.fluid.37.061903.175710>, 2005.
- Haywood, J. M. and Shine, K. P.: The effect of anthropogenic sulfate and soot aerosol on the clear sky planetary radiation budget, *Geophys. Res. Lett.*, 22, 603–606, <https://doi.org/10.1029/95GL00075>, 1995.
- Haywood, J. M., Roberts, D. L., Slingo, A., Edwards, J. M., and Shine, K. P.: General Circulation Model Calculations of the Direct Radiative Forcing by Anthropogenic Sulfate and Fossil-Fuel Soot Aerosol, *J. Climate*, 10, 1562–1577, [https://doi.org/10.1175/1520-0442\(1997\)010<1562:Gcmcot>2.0.Co;2](https://doi.org/10.1175/1520-0442(1997)010<1562:Gcmcot>2.0.Co;2), 1997.
- Haywood, J. M., Jones, A., Clarisse, L., Bourassa, A., Barnes, J., Telford, P., Bellouin, N., Boucher, O., Agnew, P., Clerbaux, C., Coheur, P., Degenstein, D., and Braesicke, P.: Observations of the eruption of the Sarychev volcano and simulations using the HadGEM2 climate model, *J. Geophys. Res.*, 115, D21212, <https://doi.org/10.1029/2010jd014447>, 2010.
- Haywood, J. M., Jones, A., and Jones, G. S.: The impact of volcanic eruptions in the period 2000–2013 on global mean temperature trends evaluated in the HadGEM2-ES climate model, *Atmos. Sci. Lett.*, 15, 92–96, <https://doi.org/10.1002/asl2.471>, 2014.
- Hedelt, P., Efremenko, D. S., Loyola, D. G., Spurr, R., and Clarisse, L.: Sulfur dioxide layer height retrieval from Sentinel-5 Precursor/TROPOMI using FP_ILM, *Atmos. Meas. Tech.*, 12, 5503–5517, <https://doi.org/10.5194/amt-12-5503-2019>, 2019.
- Hirsch, E. and Koren, I.: Record-breaking aerosol levels explained by smoke injection into the stratosphere, *Science*, 371, 1269–1274, 2021.
- Holben, B. N., Eck, T. F., Slutsker, I. A., Tanre, D., Buis, J., Setzer, A., Vermote, E., Reagan, J. A., Kaufman, Y., and Nakajima, T.: AERONET – A federated instrument network and data archive for aerosol characterization, *Remote Sens. Environ.*, 66, 1–16, [https://doi.org/10.1016/S0034-4257\(98\)00031-5](https://doi.org/10.1016/S0034-4257(98)00031-5), 1998.
- Höpfner, M., Boone, C. D., Funke, B., Glatthor, N., Grabowski, U., Günther, A., Kellmann, S., Kiefer, M., Linden, A., Losow, S., Pumphrey, H. C., Read, W. G., Roiger, A., Stiller, G., Schlager, H., von Clarmann, T., and Wissmüller, K.: Sulfur dioxide (SO₂) from MIPAS in the upper troposphere and lower stratosphere 2002–2012, *Atmos. Chem. Phys.*, 15, 7017–7037, <https://doi.org/10.5194/acp-15-7017-2015>, 2015.
- Jégou, F., Berthet, G., Brogniez, C., Renard, J.-B., François, P., Haywood, J. M., Jones, A., Bourgeois, Q., Lurton, T., Auriol, F., Godin-Beekmann, S., Guimbaud, C., Krysztofiak, G., Gaubicher, B., Chartier, M., Clarisse, L., Clerbaux, C., Balois, J. Y., Verwaerde, C., and Daugeron, D.: Stratospheric aerosols from the Sarychev volcano eruption in the 2009 Arctic summer, *Atmos. Chem. Phys.*, 13, 6533–6552, <https://doi.org/10.5194/acp-13-6533-2013>, 2013.
- Johnson, B., Turnbull, K., Brown, P., Burgess, R., Dorsey, J., Baran, A. J., Webster, H., Haywood, J., Cotton, R., Ulanowski, Z., Hesse, E., Woolley, A., and Rosenberg, P.: In situ observations of volcanic ash clouds from the FAAM aircraft during the eruption of Eyjafjallajökull in 2010, *J. Geophys. Res.-Atmos.*, 117, D00U24, <https://doi.org/10.1029/2011jd016760>, 2012.
- Johnson, J., Taha, G., Loughman, R., Zhu, T., and DeLand, M.: (GES DISC): README Document for the Suomi-NPP OMPS LP L2 AER Daily Product, https://snpp-omps.gesdisc.eosdis.nasa.gov/data/SNPP_OMPS_Level2/OMPS_NPP_LP_L2_AER_DAILY.2/doc/README_OMPS_NPP_LP_L2_AER_DAILY_v2.1.pdf (last access: 24 March 2023), 2020.
- Johnson, M. S., Strawbridge, K., Knowland, K. E., Keller, C., and Travis, M.: Long-range transport of Siberian biomass burning emissions to North America during FIREX-AQ, *Atmos. Environ.*, 252, 118241, <https://doi.org/10.1016/j.atmosenv.2021.118241>, 2021.
- Jones, A. C., Haywood, J. M., Jones, A., and Aquila, V.: Sensitivity of volcanic aerosol dispersion to meteorological conditions: A Pinatubo case study, *J. Geophys. Res.-Atmos.*, 121, 6892–6908, <https://doi.org/10.1002/2016JD025001>, 2016.
- Jones, A. C., Haywood, J. M., Dunstone, N., Emanuel, K., Hawcroft, M. K., Hodges, K. I., and Jones, A.: Impacts of hemispheric solar geoengineering on tropical cyclone frequency, *Nat. Commun.*, 8, 1382, <https://doi.org/10.1038/s41467-017-01606-0>, 2017.
- Joshi, M. M. and Jones, G. S.: The climatic effects of the direct injection of water vapour into the stratosphere by large volcanic eruptions, *Atmos. Chem. Phys.*, 9, 6109–6118, <https://doi.org/10.5194/acp-9-6109-2009>, 2009.
- Karagulian, F., Clarisse, L., Clerbaux, C., Prata, A. J., Hurtmans, D., and Coheur, P. F.: Detection of volcanic SO₂, ash, and H₂SO₄ using the Infrared Atmospheric Sounding Interferometer (IASI), *J. Geophys. Res.*, 115, D00L02, <https://doi.org/10.1029/2009jd012786>, 2010.
- Kloss, C., Berthet, G., Sellitto, P., Ploeger, F., Taha, G., Tidiga, M., Eremenko, M., Bossolasco, A., Jégou, F., Renard, J.-B., and Legras, B.: Stratospheric aerosol layer perturbation caused by the 2019 Raikoke and Ulawun eruptions and their radiative forcing, *Atmos. Chem. Phys.*, 21, 535–560, <https://doi.org/10.5194/acp-21-535-2021>, 2021.
- Kravitz, B., Robock, A., and Bourassa, A.: Negligible climatic effects from the 2008 Okmok and Kasatochi volcanic eruptions, *J. Geophys. Res.*, 115, D00L05, <https://doi.org/10.1029/2009jd013525>, 2010.
- Langmann, B.: On the Role of Climate Forcing by Volcanic Sulphate and Volcanic Ash, *Adv. Meteorol.*, 2014, 340123, <https://doi.org/10.1155/2014/340123>, 2014.
- Lawrence, M. G., Schäfer, S., Muri, H., Scott, V., Oschlies, A., Vaughan, N. E., Boucher, O., Schmidt, H., Haywood, J., and Scheffran, J.: Evaluating climate geoengineering proposals in the context of the Paris Agreement temperature goals, *Nat. Commun.*, 9, 3734, <https://doi.org/10.1038/s41467-018-05938-3>, 2018.
- Lee, K. H., Li, Z., Kim, Y. J., and Kokhanovsky, A.: Atmospheric Aerosol Monitoring from Satellite Observations: A History of Three Decades, in: *Atmospheric and Biological Environmental Monitoring*, edited by: Kim, Y. J., Platt, U., Gu, M. B., and Iwahashi, H., Springer Netherlands, Dordrecht, 13–38, https://doi.org/10.1007/978-1-4020-9674-7_2, 2009.

- Mann, G. W., Carslaw, K. S., Spracklen, D. V., Ridley, D. A., Manktelow, P. T., Chipperfield, M. P., Pickering, S. J., and Johnson, C. E.: Description and evaluation of GLOMAP-mode: a modal global aerosol microphysics model for the UKCA composition-climate model, *Geosci. Model Dev.*, 3, 519–551, <https://doi.org/10.5194/gmd-3-519-2010>, 2010.
- Mann, G. W., Carslaw, K. S., Ridley, D. A., Spracklen, D. V., Pringle, K. J., Merikanto, J., Korhonen, H., Schwarz, J. P., Lee, L. A., Manktelow, P. T., Woodhouse, M. T., Schmidt, A., Breider, T. J., Emmerson, K. M., Reddington, C. L., Chipperfield, M. P., and Pickering, S. J.: Intercomparison of modal and sectional aerosol microphysics representations within the same 3-D global chemical transport model, *Atmos. Chem. Phys.*, 12, 4449–4476, <https://doi.org/10.5194/acp-12-4449-2012>, 2012.
- McCormick, P. M., Thomason, L., and Trepte, C.: Atmospheric effects of the Mt Pinatubo eruption, *Nature*, 373, 399–404, <https://doi.org/10.1038/373399a0>, 1995.
- Millington, S. C., Saunders, R. W., Francis, P. N., and Webster, H. N.: Simulated volcanic ash imagery: A method to compare NAME ash concentration forecasts with SEVIRI imagery for the Eyjafjallajökull eruption in 2010, *J. Geophys. Res.-Atmos.*, 117, D00U17, <https://doi.org/10.1029/2011JD016770>, 2012.
- Muser, L. O., Hoshyaripour, G. A., Bruckert, J., Horváth, Á., Malinina, E., Wallis, S., Prata, F. J., Rozanov, A., von Savigny, C., Vogel, H., and Vogel, B.: Particle aging and aerosol–radiation interaction affect volcanic plume dispersion: evidence from the Raikoke 2019 eruption, *Atmos. Chem. Phys.*, 20, 15015–15036, <https://doi.org/10.5194/acp-20-15015-2020>, 2020.
- Newman, S. M., Clarisse, L., Hurtmans, D., Marenco, F., Johnson, B., Turnbull, K., Havemann, S., Baran, A. J., O’Sullivan, D., and Haywood, J.: A case study of observations of volcanic ash from the Eyjafjallajökull eruption: 2. Airborne and satellite radiative measurements, *J. Geophys. Res.-Atmos.*, 117, D00U13, <https://doi.org/10.1029/2011JD016780>, 2012.
- Niemeier, U., Timmreck, C., Graf, H.-F., Kinne, S., Rast, S., and Self, S.: Initial fate of fine ash and sulfur from large volcanic eruptions, *Atmos. Chem. Phys.*, 9, 9043–9057, <https://doi.org/10.5194/acp-9-9043-2009>, 2009.
- Niemeier, U., Riede, F., and Timmreck, C.: Simulation of ash clouds after a Laacher See-type eruption, *Clim. Past*, 17, 633–652, <https://doi.org/10.5194/cp-17-633-2021>, 2021.
- Ohneiser, K., Ansmann, A., Chudnovsky, A., Engelmann, R., Ritter, C., Veselovskii, I., Baars, H., Gebauer, H., Griesche, H., Radenz, M., Hofer, J., Althausen, D., Dahlke, S., and Maturilli, M.: The unexpected smoke layer in the High Arctic winter stratosphere during MOSAiC 2019–2020, *Atmos. Chem. Phys.*, 21, 15783–15808, <https://doi.org/10.5194/acp-21-15783-2021>, 2021.
- Osborne, M. J., de Leeuw, J., Witham, C., Schmidt, A., Beckett, F., Kristiansen, N., Buxmann, J., Saint, C., Welton, E. J., Fochesatto, J., Gomes, A. R., Bundke, U., Petzold, A., Marenco, F., and Haywood, J.: The 2019 Raikoke volcanic eruption – Part 2: Particle-phase dispersion and concurrent wildfire smoke emissions, *Atmos. Chem. Phys.*, 22, 2975–2997, <https://doi.org/10.5194/acp-22-2975-2022>, 2022.
- Peterson, D. A., Campbell, J. R., Hyer, E. J., Fromm, M. D., Kablick, G. P., Cossuth, J. H., and DeLand, M. T.: Wildfire-driven thunderstorms cause a volcano-like stratospheric injection of smoke, *npj Climate and Atmospheric Science*, 1, 30, <https://doi.org/10.1038/s41612-018-0039-3>, 2018.
- Plumb, R. A.: A “tropical pipe” model of stratospheric transport, *J. Geophys. Res.-Atmos.*, 101, 3957–3972, <https://doi.org/10.1029/95JD03002>, 1996.
- Ridley, J. K., Blockley, E. W., Keen, A. B., Rae, J. G. L., West, A. E., and Schroeder, D.: The sea ice model component of HadGEM3-GC3.1, *Geosci. Model Dev.*, 11, 713–723, <https://doi.org/10.5194/gmd-11-713-2018>, 2018.
- Robock, A.: Volcanic eruptions and climate, *Rev. Geophys.*, 38, 191–219, <https://doi.org/10.1029/1998rg000054>, 2000.
- Sellar, A. A., Jones, C. G., Mulcahy, J. P., Tang, Y., Yool, A., Wiltshire, A., O’Connor, F. M., Stringer, M., Hill, R., Palmieri, J., Woodward, S., Mora, L., Kuhlbrodt, T., Rumbold, S. T., Kelley, D. I., Ellis, R., Johnson, C. E., Walton, J., Abraham, N. L., Andrews, M. B., Andrews, T., Archibald, A. T., Berthou, S., Burke, E., Blockley, E., Carslaw, K., Dalvi, M., Edwards, J., Folberth, G. A., Gedney, N., Griffiths, P. T., Harper, A. B., Hendry, M. A., Hewitt, A. J., Johnson, B., Jones, A., Jones, C. D., Keeble, J., Liddicoat, S., Morgenstern, O., Parker, R. J., Predoi, V., Robertson, E., Siahann, A., Smith, R. S., Swaminathan, R., Woodhouse, M. T., Zeng, G., and Zerroukat, M.: UKESM1: Description and Evaluation of the U.K. Earth System Model, *J. Adv. Model. Earth Sy.*, 11, 4513–4558, <https://doi.org/10.1029/2019ms001739>, 2019.
- Shallcross, S. E.: The role of volcanic ash in the global dispersion of the aerosol cloud from major tropical eruptions, PhD thesis, University of Leeds, 2020.
- Shallcross, S., Mann, G., Schmidt, A., Haywood, J., Beckett, F., Jones, A., Neely, R., Vaughan, G., and Dhomse, S.: Long-lived ultra-fine ash particles within the Pinatubo volcanic aerosol cloud and their potential impact on its global dispersion and radiative forcings, EGU General Assembly 2021, online, 19–30 Apr 2021, EGU21-16034, <https://doi.org/10.5194/egusphere-egu21-16034>, 2021.
- Staunton-Sykes, J., Aubry, T. J., Shin, Y. M., Weber, J., Marshall, L. R., Luke Abraham, N., Archibald, A., and Schmidt, A.: Co-emission of volcanic sulfur and halogens amplifies volcanic effective radiative forcing, *Atmos. Chem. Phys.*, 21, 9009–9029, <https://doi.org/10.5194/acp-21-9009-2021>, 2021.
- Stenchikov, G., Ukhov, A., Osipov, S., Ahmadov, R., Grell, G., Cady-Pereira, K., Mlawer, E., and Iacono, M.: How Does a Pinatubo-Size Volcanic Cloud Reach the Middle Stratosphere?, *J. Geophys. Res.-Atmos.*, 126, e2020JD033829, <https://doi.org/10.1029/2020JD033829>, 2021.
- Storkey, D., Blaker, A. T., Mathiot, P., Megann, A., Aksenov, Y., Blockley, E. W., Calvert, D., Graham, T., Hewitt, H. T., Hyder, P., Kuhlbrodt, T., Rae, J. G. L., and Sinha, B.: UK Global Ocean GO6 and GO7: a traceable hierarchy of model resolutions, *Geosci. Model Dev.*, 11, 3187–3213, <https://doi.org/10.5194/gmd-11-3187-2018>, 2018.
- Taha, G.: OMPS-NPP L2 LP Aerosol Extinction Vertical Profile swath daily 3slit V2, Goddard Earth Sciences Data and Information Services Center (GES DISC) [data set], <https://doi.org/10.5067/CX2B9NW6FI27>, 2020.
- Taha, G., Loughman, R., Zhu, T., Thomason, L., Kar, J., Rieger, L., and Bourassa, A.: OMPS LP Version 2.0 multi-wavelength aerosol extinction coefficient retrieval algorithm, *Atmos. Meas. Tech.*, 14, 1015–1036, <https://doi.org/10.5194/amt-14-1015-2021>, 2021.

- Thomason, L.: Observations of a New SAGE II Aerosol Extinction Mode Following the Eruption of Mount Pinatubo, *Geophys. Res. Lett.*, 19, 2179–2182, <https://doi.org/10.1029/92GL02185>, 1992.
- Thomason, L. and Peter, T. (Eds.): SPARC assessment of stratospheric aerosol properties, SPARC Report No. 4, WCRP-124, WMO/TD-No. 1295, 2006.
- Toledano, C., González, R., Fuertes, D., Cuevas, E., Eck, T. F., Kazadzis, S., Kouremeti, N., Gröbner, J., Goloub, P., Blarel, L., Román, R., Barreto, Á., Berjón, A., Holben, B. N., and Cachorro, V. E.: Assessment of Sun photometer Langley calibration at the high-elevation sites Mauna Loa and Izaña, *Atmos. Chem. Phys.*, 18, 14555–14567, <https://doi.org/10.5194/acp-18-14555-2018>, 2018.
- Toth, T. D., Campbell, J. R., Reid, J. S., Tackett, J. L., Vaughan, M. A., Zhang, J., and Marquis, J. W.: Minimum aerosol layer detection sensitivities and their subsequent impacts on aerosol optical thickness retrievals in CALIPSO level 2 data products, *Atmos. Meas. Tech.*, 11, 499–514, <https://doi.org/10.5194/amt-11-499-2018>, 2018.
- Turnbull, K., Johnson, B., Marengo, F., Haywood, J., Minikin, A., Weinzierl, B., Schlager, H., Schumann, U., Leadbetter, S., and Woolley, A.: A case study of observations of volcanic ash from the Eyjafjallajökull eruption: 1. In situ airborne observations, *J. Geophys. Res.-Atmos.*, 117, D00U12, <https://doi.org/10.1029/2011JD016688>, 2012.
- Vaughan, G., Wareing, D., and Ricketts, H.: Measurement Report: Lidar measurements of stratospheric aerosol following the 2019 Raikoke and Ulawun volcanic eruptions, *Atmos. Chem. Phys.*, 21, 5597–5604, <https://doi.org/10.5194/acp-21-5597-2021>, 2021.
- Vernier, J. P., Fairlie, T. D., Deshler, T., Natarajan, M., Knepp, T., Foster, K., Wienhold, F. G., Bedka, K. M., Thomason, L., and Trepte, C.: In situ and space-based observations of the Kelud volcanic plume: The persistence of ash in the lower stratosphere, *J. Geophys. Res.-Atmos.*, 121, 11104–11118, <https://doi.org/10.1002/2016JD025344>, 2016.
- Visioni, D., Bednarz, E. M., Lee, W. R., Kravitz, B., Jones, A., Haywood, J. M., and MacMartin, D. G.: Climate response to off-equatorial stratospheric sulfur injections in three Earth system models – Part 1: Experimental protocols and surface changes, *Atmos. Chem. Phys.*, 23, 663–685, <https://doi.org/10.5194/acp-23-663-2023>, 2023.
- Wells, A.: awells96/Raikoke: Code for figures in “Including ash in UKESM1 model simulations of the Raikoke volcanic eruption reveal improved agreement with observations” by Wells et al., 2023, (v1.1), Zenodo [code], <https://doi.org/10.5281/zenodo.7603038>, 2023.
- Wells, A., Jones, A., Osborne, M., Damany-Pearce, L., Partridge, D., and Haywood, J.: Data for “Including ash in UKESM1 model simulations of the Raikoke volcanic eruption reveal improved agreement with observations” by Wells et al., 2023, Zenodo [data set], <https://doi.org/10.5281/zenodo.7602563>, 2023.
- Winker, D. M., Powell, K. A., Hu, Y., Omar, A., Vaughan, M. A., Liu, Z., Hunt, W. H., and Young, S. A.: Overview of the CALIPSO Mission and CALIOP Data Processing Algorithms, *J. Atmos. Ocean. Tech.*, 26, 2310–2323, <https://doi.org/10.1175/2009jtecha1281.1>, 2009.
- Woodward, S.: Modeling the atmospheric life cycle and radiative impact of mineral dust in the Hadley Centre climate model, *J. Geophys. Res.-Atmos.*, 106, 18155–18166, <https://doi.org/10.1029/2000jd900795>, 2001.
- Woodward, S.: Hadley Centre Technical Note 87 Mineral Dust in HadGEM2, https://sds-was.aemet.es/forecast-products/dust-forecasts/Woodward_2011_HadGEM2.pdf (last access: 24 March 2023), 2011.
- Woodward, S., Sellar, A. A., Tang, Y., Stringer, M., Yool, A., Robertson, E., and Wiltshire, A.: The simulation of mineral dust in the United Kingdom Earth System Model UKESM1, *Atmos. Chem. Phys.*, 22, 14503–14528, <https://doi.org/10.5194/acp-22-14503-2022>, 2022.
- Yang, K.: OMPS-NPP L2 NM Sulfur Dioxide (SO₂) Total and Tropospheric Column swath orbital V2, Goddard Earth Sciences Data and Information Services Center (GES DISC) [data set], <https://doi.org/10.5067/A9O02ZH0J94R>, 2017.
- Yool, A., Popova, E. E., and Anderson, T. R.: MEDUSA-2.0: an intermediate complexity biogeochemical model of the marine carbon cycle for climate change and ocean acidification studies, *Geosci. Model Dev.*, 6, 1767–1811, <https://doi.org/10.5194/gmd-6-1767-2013>, 2013.
- Zhu, Y., Toon, O. B., Jensen, E. J., Bardeen, C. G., Mills, M. J., Tolbert, M. A., Yu, P., and Woods, S.: Persisting volcanic ash particles impact stratospheric SO₂ lifetime and aerosol optical properties, *Nat. Commun.*, 11, 4526, <https://doi.org/10.1038/s41467-020-18352-5>, 2020.